1-1-2002

ECR plasma analysis: correlation between plasma conditions and growth rate

Marsela Pontoh
Iowa State University

ECR plasma analysis: Correlation between plasma conditions and growth rate

by

Marsela Pontoh

A thesis submitted to the graduate faculty

in partial fulfillment of the requirements for the degree of

MASTER OF SCIENCE

Major: Electrical Engineering

Program of Study Committee:
Vikram Dalal (Major Professor)
Gary Tuttle
David Lynch

Iowa State University

Ames, Iowa

2002

Graduate College
Iowa State University

This is to certify that the master's thesis of

Marsela Pontoh

has met the thesis requirements of Iowa State University

Signatures have been redacted for privacy

To my parents .....
whose love, support and encouragement
have made this possible

TABLE OF CONTENTS

ABSTRACT

A spectroscopic study of electron cyclotron-resonance (ECR) plasma was conducted to correlate amorphous and microcrystalline Si film growth rate with plasma properties. Optical emission spectroscopy (OES), mass spectroscopy (MS), and Langmuir probe were used to perform plasma analysis. We found that the addition of hydrogen into a helium-silane plasma, immediately reduces the amount of SiH_x (x = 0-3) radicals and ions as well as the film growth rate. The decrease in growth rate was shown to be linear with the decrease in SiH emission count. Adding hydrogen increases the etch rate by H ions and reduces the formation of the radical responsible for growth. Surprisingly, we found that the concentration of SiH_3 is comparable to or lower than the concentration of SiH. This observation raises a question about how well the standard silicon growth model fits the data from ERC systems. In this work we also shows that radical and ion formation increases linearly with microwave power. On the other hand, the increase in chamber pressure reduces ion formation. Emission intensity ratio, H_α to H_2, decreases with pressure. This means that at low pressure more H ions are available for etching, thus promoting the growth of a microcrystalline film.

CHAPTER 1. INTRODUCTION

It has been known for over a century that an electrical discharge in gasses promotes chemical reactions [1]. However, only during the last couple of decades has plasma deposition become an important technique in the chemical industry. The rapid improvement in plasma technology was promoted by the material requirements in microelectronics, optics and solar energy research.

There are various types of discharges present today. Among those are glow (DC) discharge, RF discharge, magnetron discharge, and microwave discharge. In magnetron discharge, the plasma is initiated by a DC or RF source. The magnetic field is used to cause the paths of the electrons to form a closed loop. This increases the electron confinement and produces a higher plasma density. A similar idea is applied in the electron cyclotron-resonance chemical vapor deposition (ECR-CVD) system used in this work. In the ECR-CVD system, the plasma is generated by a microwave power source. The microwave energy is then coupled with the resonant frequency of the electron gas in the presence of a static magnetic field.

The use of an ECR discharge is important in low-temperature and low-pressure plasma processing. Some of the advantages of using an ECR plasma include

1. ability to control plasma potential;
2. ability to produce high density of excited species;
3. ability to operate at low pressure;
4. ability to have an enhanced growth rate at low temperature;
5. minimum substrate damage from ion bombardment; and
6. ability to utilize a low-cost microwave power supply.

The drawbacks of the ECR system include

1. the use of magnetic field which makes it more difficult to control; and
2. the difficulty to scale up due to the complexity of the system.

1.1 Amorphous Silicon

Hydrogenated amorphous silicon has attracted the interest of many researchers due to its potential application in various devices. a-Si:H has been used in transistors, flat panel displays [2], detector [3], solar cells [4-6] and many other electrical and optical devices. The a-Si:H solar cell is one of the promising candidates for clean energy source. One of the challenges to enable this solar energy device to compete with other alternative energy sources is to reduce the production cost. Much of the current a-Si:H solar cell research is aimed at the reduction of production costs and improvement of the cell efficiency and stability [5]. One way of reducing the production costs can be achieved by increasing the deposition rate.

Silane or silane-containing discharges has been used to produce a-Si:H solar cells. Much research has been conducted to study the growth mechanism of a-Si:H. Understanding the growth mechanism is essential for a growth rate study. Growth models have been developed to determine the radical species responsible for growth. It is believed that the silyl radical, SiH_3, is responsible for both growth and creation of growth sites [7].

1.2 Objective of Study

While an ECR plasma has been successfully used to grow high quality a-Si:H [4,8], little has been known on the relationship between growth rates and fundamental plasma

properties. The objective of this research is to investigate the properties of ECR discharge using in-situ OES and MS, to develop a correlation between a:Si-H film growth rate and plasma properties and to determine which radicals play a role in the growth of a:Si-H. OES, MS and Langmuir probe measurements were conducted to collect emission intensity, ion concentration and electron energy data on various plasma conditions. a-Si:H films, grown in a $He-H_2-SiH_4$ plasma, were then used to study the growth rate. We wish to show that is possible to control the growth rate by monitoring the plasma properties.

CHAPTER 2. ECRCVD

2.1 Fundamentals of Plasma

A plasma is a partially ionized gas. Because of the light given off by the plasma, it is often called "glow discharge". Within the plasma there is a balance between positive and negative charges in macroscopic volume and time. Therefore a plasma is usually considered to be quasineutral.

Plasma can be categorized into two large groups: nonequilibrium (nonisothermal or "cold") and equilibrium (isothermal or " thermal") plasmas. Nonequilibrium plasmas are generated at low pressure (0.5-500 mTorr) by applying a static or radio frequency field. In a nonequilibrium plasma, the free electrons have high energies (1-10 eV). However, neutrals and ions have low energies (a few hundredths of eV) because of their large mass. Due to the difference in their energy, electrons have a high temperature (50,000K) while neutrals and ions have low temperature (500K). Under nonequilibrium conditions, the initiation reaction occurs by collisions with the "hot" electrons, which results in a lower processing temperature compared to conventional processing using similar chemistry. On the other hand, in a thermal plasma, all species have the same temperature due to the shorter mean free path and higher collision frequency [9].

To better understand plasma, let us consider a simple discharge chamber. Figure 2.1 illustrates a typical DC chamber. The chamber is evacuated and filled with discharge gas. Then a DC potential is applied across the electrodes (cathode and anode). The cathode is positively charged and the anode is negatively charged. This potential difference causes an electric field going from cathode to anode. The free electrons in the discharge are accelerated by the electric field toward the cathode. Because of the small mass of the electron, it will be

affected the most. Therefore, electrons will absorb the majority of the energy from this field. Subsequently, the energetic electrons will collide with gas atoms. This collision results in momentum transfer, ionization, excitation or dissociation, depending on the energy of electron. During ionization, an electron collides with an atom or molecule, producing an ion and two electrons. These two electrons can collide with other atoms or molecules to produce more ions and electrons. The density of ions and electrons increases as a result of the above chain reaction. Finally, "breakdown" will occur when the degree of ionization exceeds a certain threshold value.

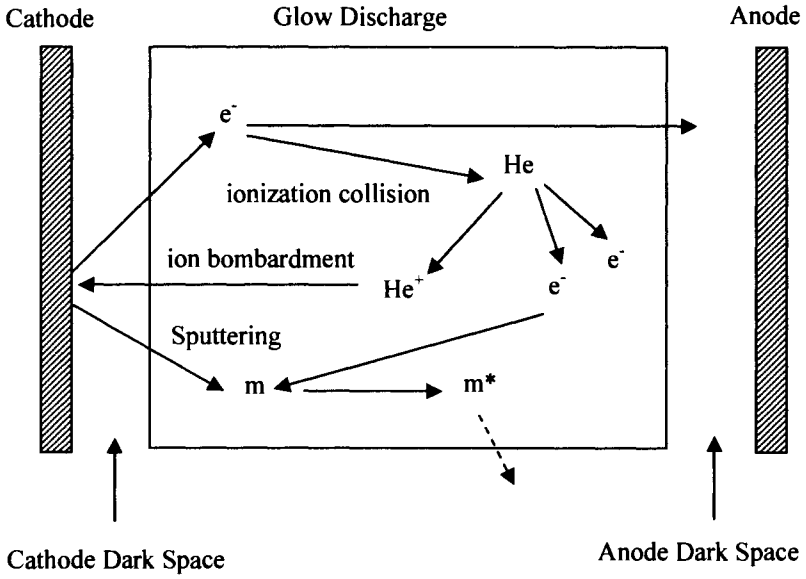

Figure 2.1. Schematic of DC Glow Discharge.

While the electrons are produced as a result of an ionization reaction, the electrons are also lost rapidly through electron-ion and electron-wall recombination. The plasma is held in continuously by counterbalancing the creation and the loss rates of electrons. As shown in

Fig. 2.1, the ion bombardment at the cathode causes the ejection of cathode atoms and electrons from the cathode surface. These electrons are called secondary electrons and are needed to maintain the discharge [10], and [11].

Between the quasineutral ($n_i = n_e$) plasma and the wall, there is a thin positively charged layer called a sheath. To understand why the sheath exists, let us consider plasma that is confined between two grounded walls. Within the plasma, the net charge density is zero. Thus the electric potential and electric field are also zero. Due to its smaller mass, the thermal velocity of electrons is at least 100 times the thermal velocity of ion. The fast-moving electrons are rapidly lost to the wall, resulting in the net positive ion sheath near each wall. Within the sheath, $n_i >> n_e$, leading to a net positive charge density. The resulting potential profile is shown in Fig 2.2. The potential difference between the plasma and the wall is often called the "plasma potential" [12].

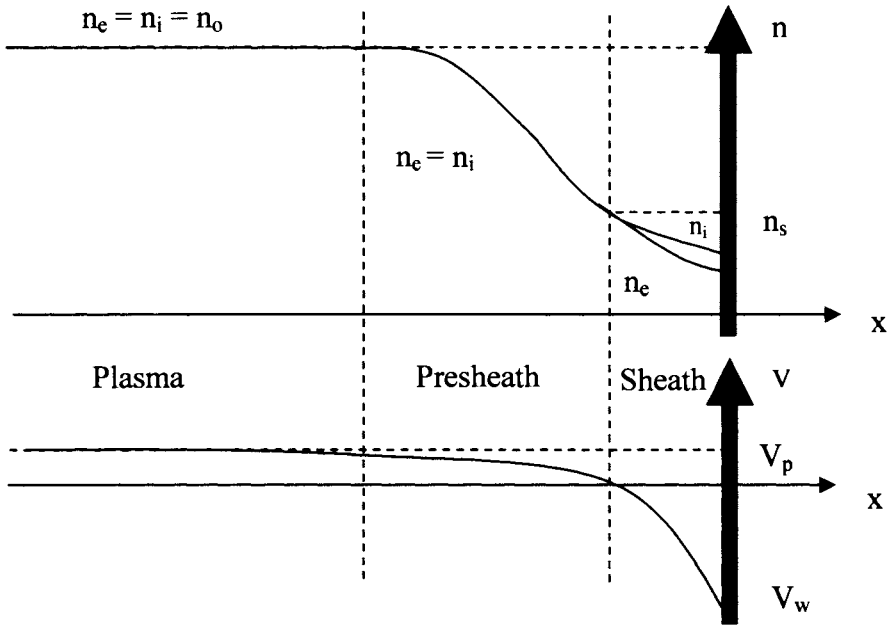

Figure 2.2. Plasma Sheaths: (a) densities, and (b) potential profile [12].

2.2 ECR Discharges

An ECR Plasma source was first used for a spacecraft propulsion application in the early 1960s. Plasma electrons are created at high magnetic field and are accelerated along the field lines towards the exhaust by the magnetic gradient force. The ECR source was used due to its high plasma density and low-pressure capability [13].

For semiconductor applications, the ECR discharge is attractive due to the high plasma density, low plasma potential, low deposition pressure and low deposition temperature. The ECR discharge is used for etching and depositing thin layer of oxides and metals.

In this section, we will review the basics of ECR discharges and then discuss the ECR system used for this research.

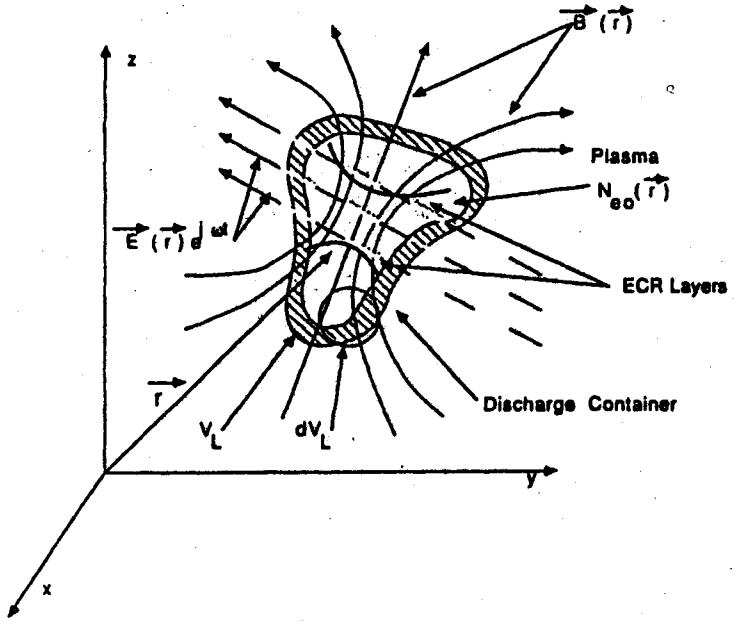

Figure 2.3. Microwave discharge of volume V_L [14].

Figure 2.3 shows a diagram of a microwave discharge that occupies a finite volume, V_L, and is bounded by the container wall. Although a plasma is considered to be neutral on the whole, the discharge of volume V_L consists of electrons, ions and neutral gases. A time and spatially varying microwave field $E(r)e^{j\omega t}$ is responsible for maintaining the discharge. As the electric field penetrates the discharge, a spatially varying magnetic field is also impressed on the discharge. The Lorentz force causes electrons in the discharge area to spiral around the static magnetic field lines. The Lorentz force is given by

$$\vec{F} = q(\vec{r} \times \vec{B}) \tag{2.1}$$

and the radius of the spiral is given by

$$R = \left(\frac{m_e}{qB}\right)\sqrt{v_x^2 + v_y^2} \tag{2.2}$$

Figure 2.4 illustrates the electron motion in static magnetic field at zero electric field and at $E = Eo\, e^{j\omega t}$ under resonance the condition.

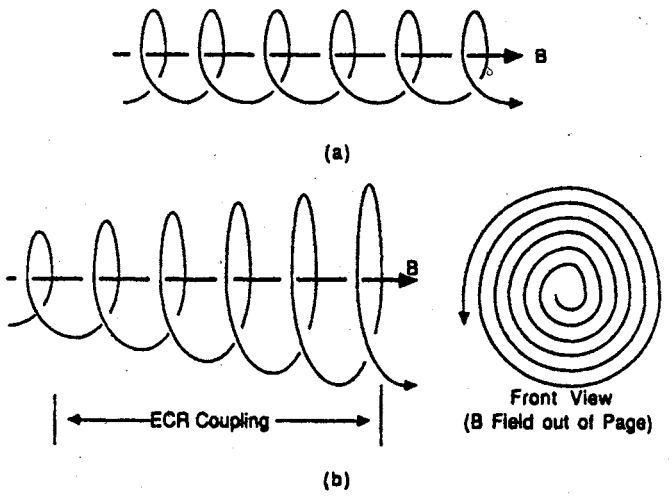

Figure 2.4. Electron motion in static magnetic field under (a) zero electric field, and (b) resonance condition [14].

When the rotation frequency, ω_e, matches the microwave frequency, ω, the resonance condition is met. The magnetic field lines (the solid-curved lines in Fig. 2.3) show the area where $\omega = \omega_e$ [14]. The rotation (cyclotron) frequency can be derived from equation 2.1 [15]. Assuming that $B = B_0 \cdot \mathbf{z}$, the cyclotron frequency is

$$\omega = \frac{qB}{m_e} \tag{2.3}$$

where B is the magnetic field intensity in tesla, and m_e is the mass of an electron.

The resonance condition can be met by tuning the magnetic field so that the free electrons are rotating in phase with the electric field of the incoming microwaves. The linearly polarized incoming microwaves can be broken up into two circularly polarized waves: the right-hand circular polarized wave (RCP), and the left-hand circular polarized wave (LCP). Equation 2.4 shows the general form of the linearly polarized wave. The first term represents RCP and the second represents LCP.

$$E = \mathrm{Re}\left[\frac{E_0}{2}(a_y + ja_x)e^{j\omega t} + \frac{E_0}{2}(a_y - ja_x)e^{j\omega t}\right] \tag{2.4}$$

At resonance, the RCP is in phase with the electrons, while the LCP is rotating in the opposite direction. However, when the plasma reaches some critical density, N_{cr}, the LCP is no longer able to propagate. Therefore RCP is the one that accelerates the free electrons and it is also responsible for the dissociation and ionization of gas molecule [15].

The critical density is given by

$$N_{cr} = \frac{\omega^2 \varepsilon_0 m_e}{q^2} \tag{2.5}$$

For 2.45 GHz microwaves used in this research, the critical density is 7.5×10^{10} cm^{-3} [15].

2.3 Description of Reactor

The ECR System used for this research is shown in Fig. 2.5. It consists of a microwave generator, a plasma chamber, two magnets, a process chamber and a vacuum system. The plasma chamber is made of a stainless steel tube and it is surrounded by two copper wire wound magnets. These magnets are controlled by two separate power supplies. A restricting orifice separates the process chamber from the plasma chamber. A substrate holder, substrate heater and a gate valve are parts of the process chamber. The vacuum system consists of a roughing pump, a turbo pump and a roots pump.

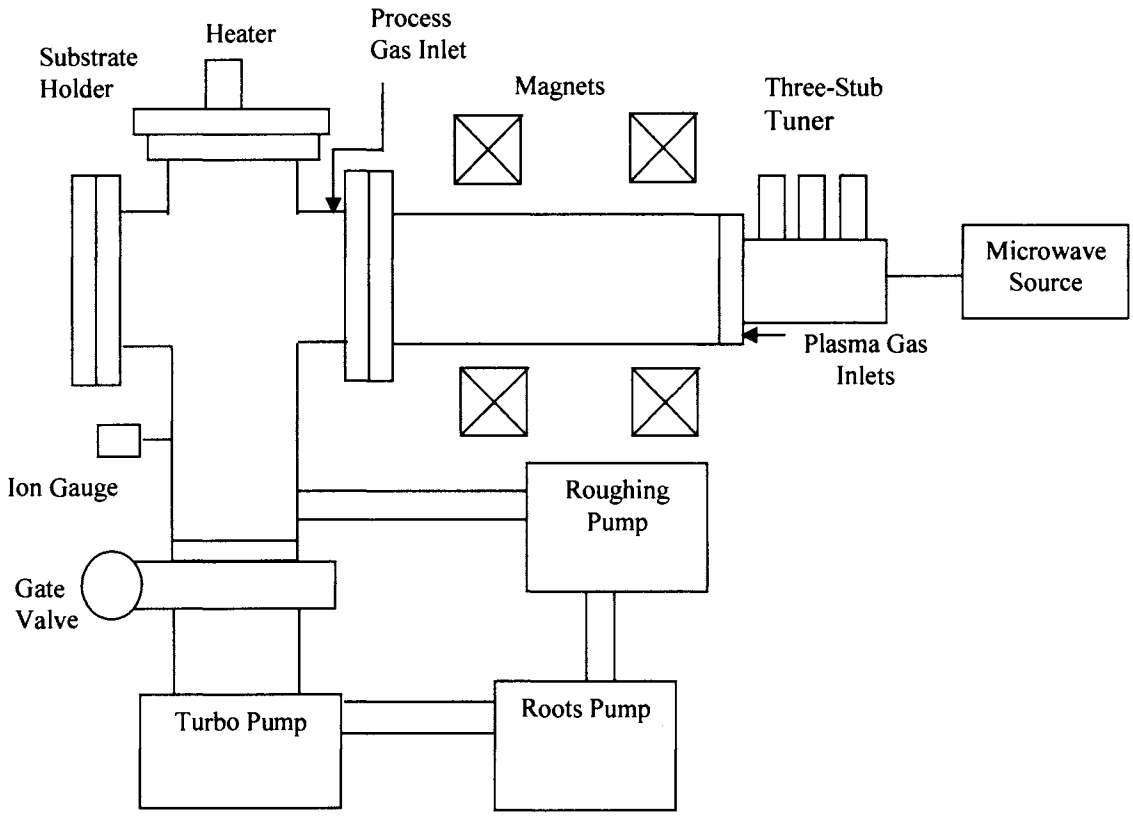

Figure 2.5. Schematic of the ERC system.

Microwaves are introduced to the chamber through a waveguide, three-stub tuner and quartz window. The microwave frequency is 2.45 GHz, which is commonly used in most ECR systems. The three-stub tuner is used to match the impedance between the waveguide, and the plasma. The two magnets are arranged in Helmholtz-coil configuration, which gives a uniform magnetic field in the z direction (the same direction as the microwaves propagate). A DC power is used to supply current to the magnets. The position of magnets with respect to other system elements is shown in Fig. 2.6.

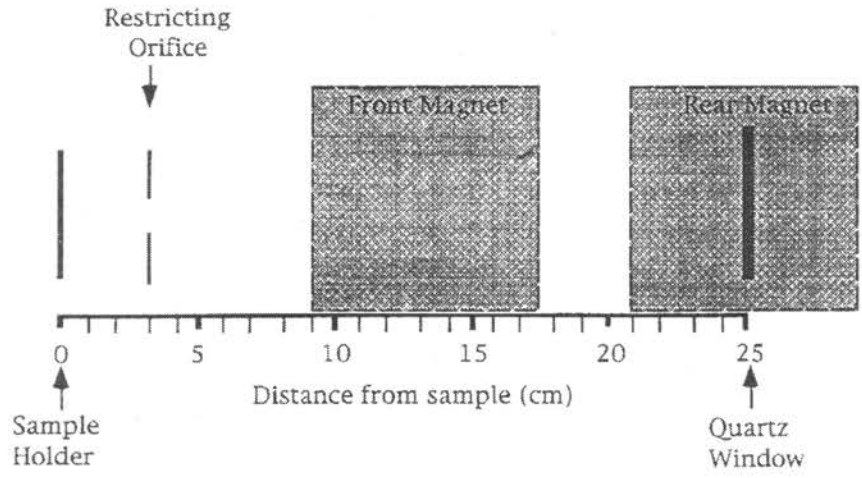

Figure 2.6. Position of magnets with respect to other system elements.

The substrate is mounted on the substrate holder and is held by the stainless steel mask. The substrate holder is made of inconel to allow high temperature operation. Heat is provided by the heating elements that are fitted inside the sample holder. The heater temperature is controlled by a Watlow temperature controller. Flowing water is used to cool the chamber wall. Plasma gases are introduced from the rear of the chamber, while the process gases are introduced close to the substrate. Gas flows are set by unit instrument

mass-flow controller. The process chamber pressure is controlled by a manual gate valve. A roughing pump is used to pump down the chamber from atmospheric pressure. Then the chamber is brought to vacuum by using a Pfeiffer turbo molecular pump. A rootes pump is connected to the outlet of the turbo pump to increase the flow rate. The exhaust gas is then diluted with nitrogen before being release into the duct.

2.4 Process Parameters

As stated earlier, the purpose of this experiment is to characterize plasma based on plasma parameters and to correlate it to the growth rate of amorphous silicon. To minimize variation among substrates, all substrates used were cleaned using identical cleaning procedure. Corning 7059 glass substrates were bought from the manufacturer and were cleaned before being loaded into the chamber. The samples were triple rinsed in DI water to remove large particles. Then they received a supersonic bath for 15 minutes. Finally, the samples were triple rinsed again in DI water before they were immersed in methanol until they were loaded.

Process parameters that can be varied during the deposition include gas selection and dilution, chamber pressure, substrate temperature, microwave power, and magnet profiles. Magnet profiles can be varied by tuning the three-stub tuner and changing the magnet currents. However, to increase the reproducibility of the plasma conditions, the magnet currents and the three-stub tuner have been optimized to give minimum reflected microwave power. They have been set so that the reflected power is less than 10 percent of the incident power. Small variations of these magnet currents and tuner settings will drastically change the plasma conditions.

The microwave power can be varied to control electron and ion energy in the plasma. Higher microwave power gives higher kinetic energies, which result in higher reaction rates to produce more radicals. Substrate temperature affects the diffusion and mobility of the atoms or molecules. Higher temperature provides more energy for the deposited atoms or molecules to diffuse and to seekout the preferred bonds. This results in higher crystallinity of films. Chamber pressure can be adjusted to control the particle density levels in the chamber. Chamber pressure can also be used to determine the mean free path of a particle or molecule. Mean free path is defined as the average distance that the particle can travel before it collides with another particle. Assuming ideal gas conditions, the mean free path is given by

$$\lambda = \frac{RT}{\sqrt{2}\pi d^2 nP} \tag{2.6}$$

where R is Reynold's number, T is temperature, P is chamber pressure, V is chamber volume and d is the particle's diameter. As pressure increases, the mean free path decreases and the growth rate decreases. Finally, gas selection and dilution will determine the types and compositions of ion and radicals produced. The concentration of ions and radicals in the plasma will affect the growth rate and alter the composition of the deposited film.

2.5 Plasma Chemistry

Growth chemistry in a plasma chamber is a complex process since several chemical reactions can occur at the same time. More and more species are generated over a period of time. To better understand the growth chemistry, we must look at the dissociation mechanism of the process gas. Figure 2.7 shows an oversimplified graphical representation

of plasma generation and particle interactions. It shows dissociation, ionization and recombination reactions between electrons, molecules, and ions.

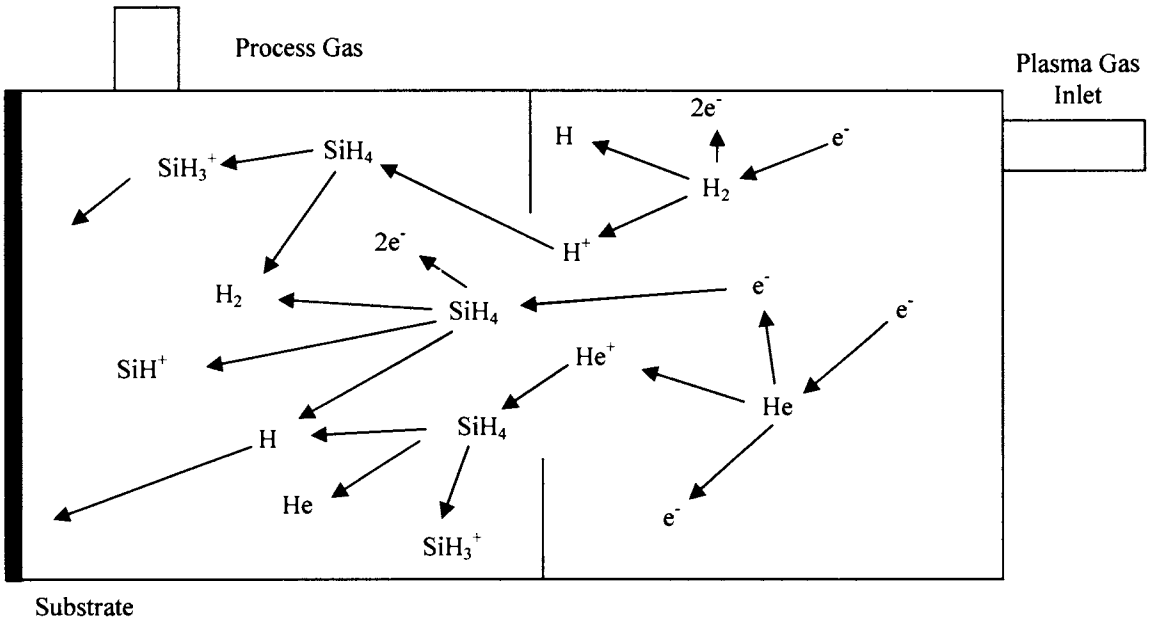

Figure 2.7. Illustration of plasma generation and chemical reactions in the process chamber.

Table 2.1. Electron impact reactions

(E1)	$e^- + H_2 \rightarrow e^- + 2H$
(E2)	$e^- + H_2 \rightarrow 2e^- + H + H^+$
(E3)	$e^- + H \rightarrow 2e^- + H^+$
(E4)	$e^- + H_2 \rightarrow 2e^- + H_2^+$
(E5)	$e^- + H_2^+ \rightarrow e^- + H^+ + H$
(E6)	$e^- + H_2^+ \rightarrow H + H^*$
(E7)	$e^- + He \rightarrow 2e^- + He^+$
(E8)	$e^- + He \rightarrow e^- + He^*$
(E9)	$e^- + SiH_4 \rightarrow SiH_3 + H + e^-$
(E10)	$e^- + SiH_4 \rightarrow SiH_2 + H_2 + e^-$
(E11)	$e^- + SiH_4 \rightarrow SiH + H_2 + H + e^-$
(E12)	$e^- + SiH_4 \rightarrow Si + 2H_2 + e^-$
(E13)	$e^- + SiH_4 \rightarrow SiH^* + H_2 + H + e^-$
(E14)	$e^- + SiH_4 \rightarrow SiH^+ + H_2 + H + 2e^-$
(E15)	$e^- + SiH_3 \rightarrow SiH_2 + H + e^-$

Table 2.2. Gas phase reactions

(G1)	$H_2 + H^+ \rightarrow H^+ + 2H$
(G2)	$H_2 + H^+ \rightarrow H_2^+ + H$
(G3)	$H^+ + 2H_2 \rightarrow H_3^+ + H_2$
(G4)	$H_2^+ + H_2 \rightarrow H_3^+ + H$
(G5)	$H + H_2 \rightarrow e^- + H + H_2^+$
(G6)	$He + H_2 \rightarrow HeH^+ + H$
(G7)	$He^+ + H_2 \rightarrow He + H_2^+$
(G8)	$He^+ + H_2^+ \rightarrow He + H + H^+$
(G9)	$He + H_2 \rightarrow He + H + H^*$
(G10)	$H^+ + He \rightarrow H + He^+$
(G11)	$H + He \rightarrow H + He^+ + e^-$
(G12)	$HeH^+ + H_2 \rightarrow H_3^+ + He$
(G13)	$SiH_4 + H \rightarrow SiH_3 + H_2$
(G14)	$SiH_4 + SiH \rightarrow Si_2H_5$
(G15)	$SiH_4 + SiH_2 \rightarrow Si_2H_6$
(G16)	$SiH_3 + SiH_3 \rightarrow Si_2H_6$
(G17)	$SiH_2+ + SiH_4 \rightarrow SiH_3 + SiH_3^+$
(G18)	$SiH_2 + H_2 \rightarrow SiH_4$
(G19)	$SiH_4 + H^+ \rightarrow SiH_3^+ + H_2$
(G20)	$SiH_4 + He^+ \rightarrow SiH_3^+ + He + H$

Table 2.3. Surface reactions

(S1)	$H + s \rightarrow H.s$	(chamber wall recombination)
(S2)	$SiH_3 + s \rightarrow SiH_3.s$	(SiH_3 adsorption)
(S3)	$SiH_2 + s \rightarrow SiH_2.s$	(SiH_2 adsorption)
(S4)	$SiH + s \rightarrow SiH.s$	(SiH adsorption)
(S5)	$Si + s \rightarrow Si.s$	(Si adsorption)
(S6)	$s.H + SiH_3 \rightarrow SiH_4 + s$	(H-abstraction by SiH_3)
(S7)	$s.H + H \rightarrow H_2 + s$	(H-abstraction by H atom)
(S8)	$SiH_3.s1 + SiH_2.s2 \rightarrow SiH_2.s1 + SiH_3.s2$	(H diffusion)
(S9)	$SiH_3.s1 + s2 \rightarrow SiH_3.s2 + s1$	(SiH_3 diffusion)
(S10)	$H.s1 + H.s2 \rightarrow H_2 + s1 + s2$	(recombination of adjacent hydrogen atoms)

Table 2.1 lists various electron impact reactions of helium, hydrogen and silane. Table 2.2 provides a partial list of gas phase reactions between molecules, ions and radicals. It gives a general idea of possible reaction mechanisms. Finally, Table 2.3 shows surface

reactions such as adsorption, diffusion and desorption. The "*" symbols in Tables 2.1 and 2.2 denote an excited state.

As can be seen from Table 2.2, the gas phase reactions can be very complex. However, it has been widely accepted that the SiH_3 radical is the primary precursor for film grown under CVD-like conditions. Experimental [16], [17] and numerical [18] studies have shown that SiH_3 radicals are the most preferable monomer radical in glow and RF discharges. Although SiH_3 can be produced by reactions E9, G13, G17, G19, G20 and other second order reactions, the dominant mechanisms are G13 and G19. Silane decomposition by the hydrogen radical selectively produces SiH_3, while plasma decomposition of silane generates all variety of radicals [19]. Gallagher [7] showed that in silane glow discharges, film growth from SiH_2 and SiH_4 radicals gave poor a-Si-H quality. This agrees with what Kawase *et al.* found [19]. According to Kawase *et al.*, polymerized radicals that contribute to the film growth were originally formed by the insertion of SiH_2 radicals into silane [19]. It is well known that polymerized radicals produce non-uniform films with low quality.

Using SiH_3 as the primary precursor for the film formation, a simple model of gas phase incorporation into an a:Si-H film is shown in Fig. 2.8. Figure 2.8(a) shows that the reaction begins with the creation of dangling bond via H-abstraction (reaction S6). Then the dangling bond diffuses to find a lower energy site (Fig. 2.8(b), reaction S8). A silyl radical is preferentially adsorbed at the high point on the film surface (Fig. 2.8(c), reaction S2). Finally, the new adsorbed radical diffuses to the nearest dangling bond (Fig. 2.8(d), reaction S9). Deposition and etching can also occur between the radical species and chamber wall. S1 represents the recombination of the radical species with the chamber wall, while S6 represents chamber wall etching by radical species.

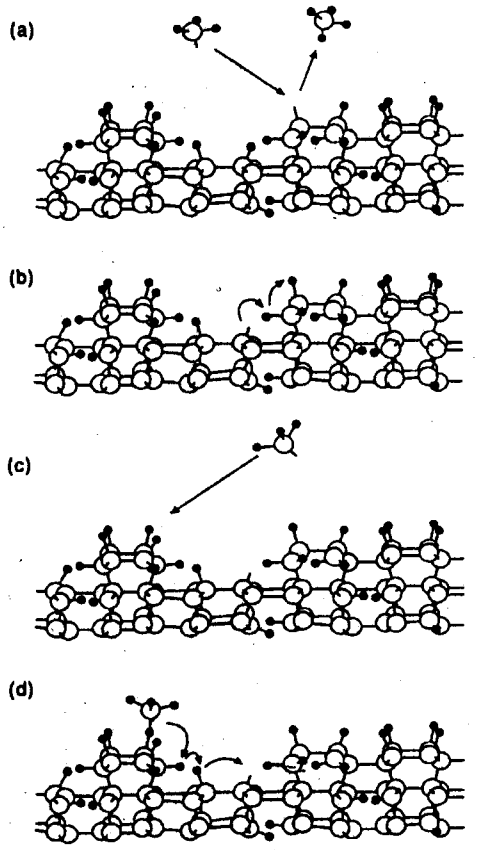

Figure 2.8. Incorporation of gas phase radical into a:SiH_4 film.
(a) Dangling bond creation. (b) Dangling bond diffusion. (c) Radical adsorption. (d) Surface diffusion of the adsorbed species [7]

CHAPTER 3. CHARACTERIZATION TECHNIQUES

3.1 Optical Emission Spectroscopy

For this research, optical emission spectroscopy (OES) is used to measure spectra emitted by the plasma. The arrangement of the OES system used in this experiment is shown in Fig. 3.1a. This OES system consists of a photon counter, a monochromator, and a controller (computer). The photon counter used is the Acton Research Corporation (ARC) PD-473-1. It consists of a photomultiplier tube detector, high voltage power supply, amplifier, discriminator, and TTL logic level converter. It has a spectral response from 185 to 850 nm with typical dark count of 80 cps, but tested to have 44.9 cps. A schematic diagram of the photon counter is shown in Fig. 3.1b.

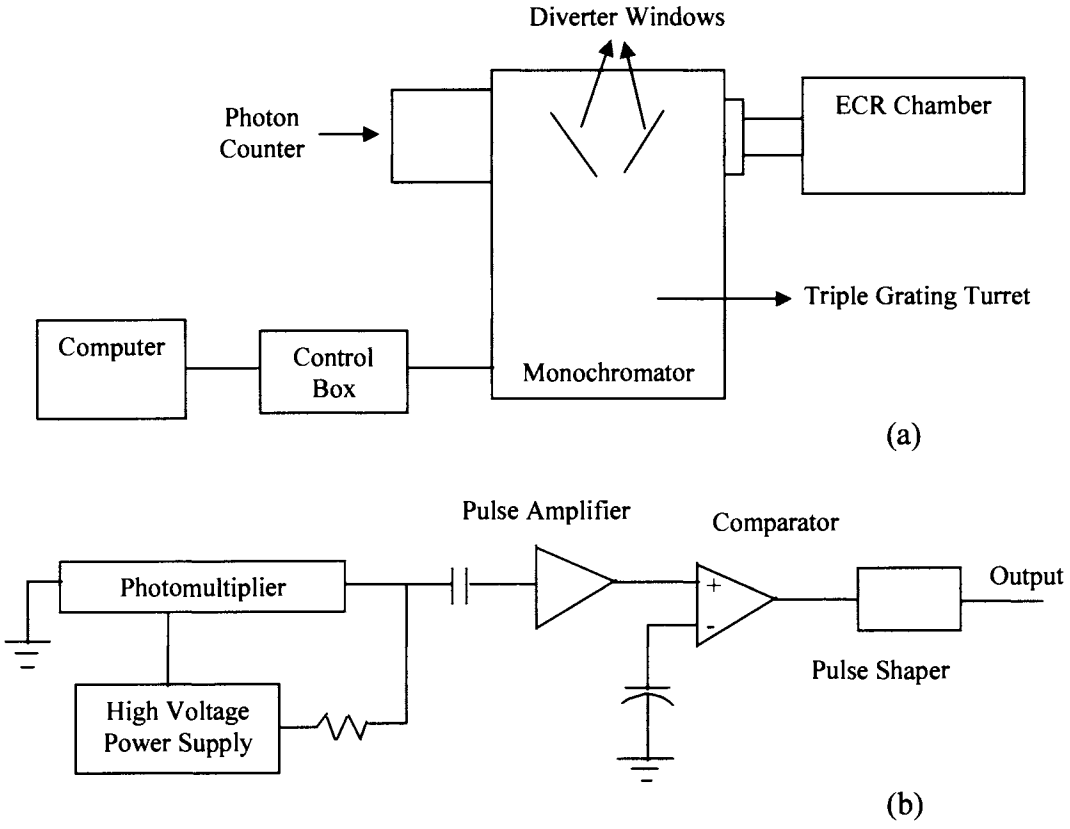

Figure 3.1. (a) OES system diagram and (b) PD-743-1 Photon Counter Diagram [20].

The monochromator is an ARC spectraPro-300i with a 1200 g/mm grating, 300 mm focal length, f/4 aperture ratio and 0 to 1400 nm scan length. The entrance and exit slits are adjustable from 10 μm to 3 mm wide. The control box is an ARC NCL electronic interface and is connected to a computer through an RS232 port. The ARC SpectraPro Monochromator Software was installed to allow PC control of the monochromator using the SpectraDrive Scan Controller.

This OES System was used to measure plasma densities by detecting the intensity of light emitted by the plasma. As we know from physics and chemistry, every element has a unique number of electrons. Each electron occupies a certain orbit or shell. Each shell represents the potential energy of the electrons within it. The allowed radius of orbits is different for every element. Therefore electrons from different elements have different energies. This fact is used to distinguish elements based on their optical spectra.

A higher energy level is represented by a larger shell radius. When an electron absorbs energy from light, it can be raised to the higher energy level. On the other hand, an electron can move to lower energy level by giving off a photon (emitting light). The energy of the emitted photon is equal to the difference in energy of the two levels. This energy is unique for every element.

In a plasma, the interaction between atoms and molecules can cause an electron to be raised or excited to a higher level. This excitation results in an opening at the lower energy level. When an electron from a higher energy level moves to fill the opening, it emits a photon which is characteristic of that particular transition. The emitted photon travels through the monochrometer and is detected by the photon counter. The energy of the photon is calculated based on the wavelength of the detected photon.

Figure 3.2 illustrates atomic transition between two energy levels (e.g. between energy level 1 and level 2). The probability of each transition illustrated in Fig. 3.2 can be expressed in the form of Einstein's coefficient B_{12} for absorption, A_{21} for spontaneous emission, and B_{21} for stimulated emission [21]. The intensity of spontaneous emission is given by

$$I_{sp} = A_{21} h\upsilon_{21} N_2 \tag{3.1}$$

Under thermal equilibrium, the number of atoms in the excited state, N_j, follows the Boltzmann distribution

$$N_j = N_0 \frac{g_j}{g_0} \exp\left[\frac{-(E_j - E_0)}{kT}\right] \tag{3.2}$$

where N_0 is the total number of atoms present ($N_0 = \sum_j N_j$), E_j is the energy of level j, and g_j is the degeneracy of the j^{th} state. Substituting 3.2 into 3.1 gives

$$I_{sp} = A_{21} h\upsilon_{21} N_0 \frac{g_2}{g_0} \exp\left[\frac{-(E_2 - E_0)}{kT}\right] \tag{3.3}$$

At equilibrium, the ratio of stimulated emission to spontaneous emission is given by

$$R = \frac{I_{st}}{I_{sp}} = \frac{1}{\exp\left(\frac{h\upsilon}{kT}\right) - 1} \tag{3.4}$$

Therefore, the intensity of stimulated emission is

$$I_{st} = A_{21} h\upsilon_{21} N_0 \frac{g_2}{g_0} \exp\left[\frac{-(E_2 - E_0)}{kT}\right] \left[\frac{1}{\exp\left(\frac{h\upsilon}{kT}\right) - 1}\right] \tag{3.5}$$

Equations 3.3 and 3.5 show that the intensity of the emitted photon is proportional to the number of atoms present in the system. The number of atoms and ions present in the system

changes as the plasma parameter changes. The relative change of the ions present in the system can be determined by the change in the OES signal.

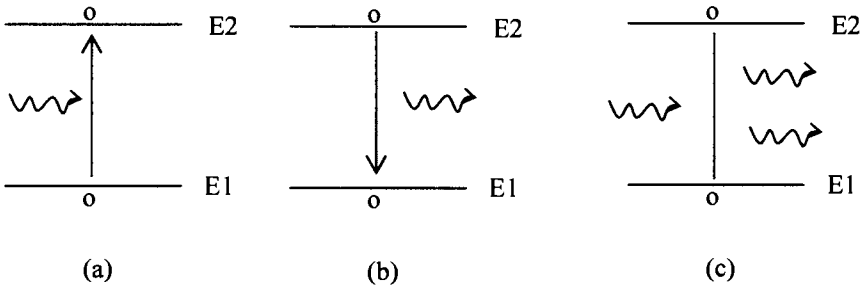

Figure 3.2. (a) Absorption, (b) Spontaneous emission, and (c) Stimulated emission.

3.2 Mass Spectrometry

Mass spectrometry (MS) is used to measure the partial pressure of ions present in the plasma. The schematic diagram of the mass spectrometer used for this research is shown in Fig. 3.3. The system consists of a closed ion source (CIS) analyzer, an electronic control unit (ECU) box, a heater jacket, a vacuum system, and a computer system. The CIS system used is a Stanford Research System (SRS) CIS200, capable of detecting ions mass up to 200 amu. The CIS is enclosed in a Conflat tee as shown in Fig. 3.4(a). The CIS probe is mounted to the back port. The front port is connected to the plasma chamber through a gate valve, and the bottom port is connected to the vacuum system. The ECU connects directly to the probe's feedthru-flange through its front panel. A computer system is connected to the rear panel of the ECU by an RS232 connector. The ECU has a built in power module for AC operation. This eliminates the need for an external DC power supply. The vacuum system used consists of a turbomolecular pump and a diaphragm pump. With the above vacuum

system, the CIS can operate up to 10^{-5} mbar. At higher pressure, the response time becomes non-linear so that a pressure reduction system placed between the plasma chamber and the CIS analyzer is needed.

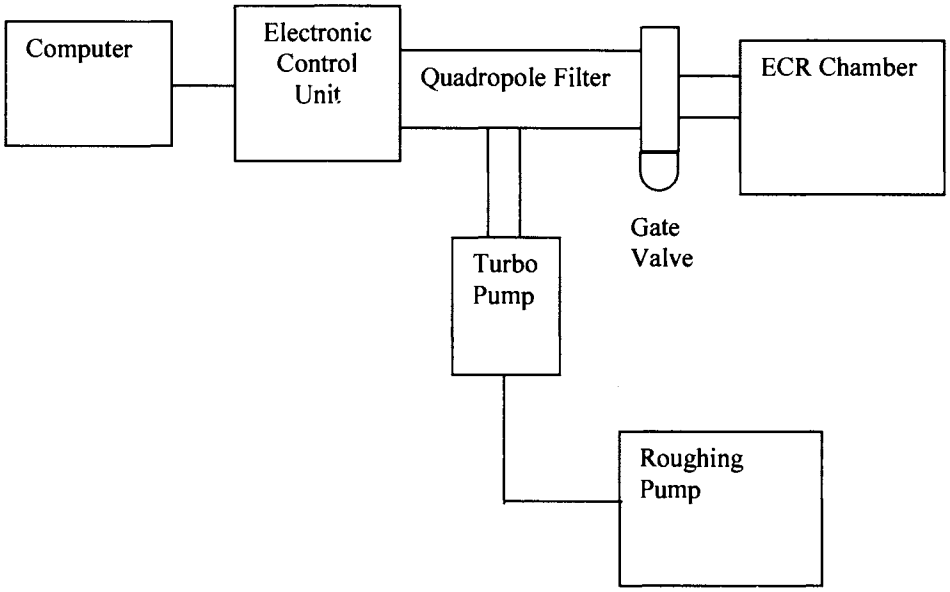

Figure 3.3. Schematic of the MS system.

The bakeout of the CIS probe is needed after the installation of the probe in the vacuum chamber and after any long exposure to open air. The bakeout accelerates the outgassing rates of molecules (especially H_2O) from the walls. A bakeout also helps clean the probe from deposits. The presence of deposits increases the contribution of the quadrupole sensor to the background signal. An electrostatic charge present on the contaminated surface effects the probe sensitivity and resolution. Therefore, when background contamination is present or when the performance of the CIS degraded, a probe bakeout is also necessary.

The CIS analyzer consists of three major parts: the closed ionizer, the quadrupole mass filter and the ion detector. Figure 3.4(b) shows the schematic of the CIS analyzer. The ionizer used is called the closed ion source (CIS). Electrons from the heated filament collide with gas molecules to produce positive ions. The ions then travel through the mass-filter where they are separated based on their mass to charge ratio [22]. In this research, the filament is turned off to allow detection of plasma ions only. By turning off the filament, we eliminate the contribution of ions produced by electron bombardment in the ionizer.

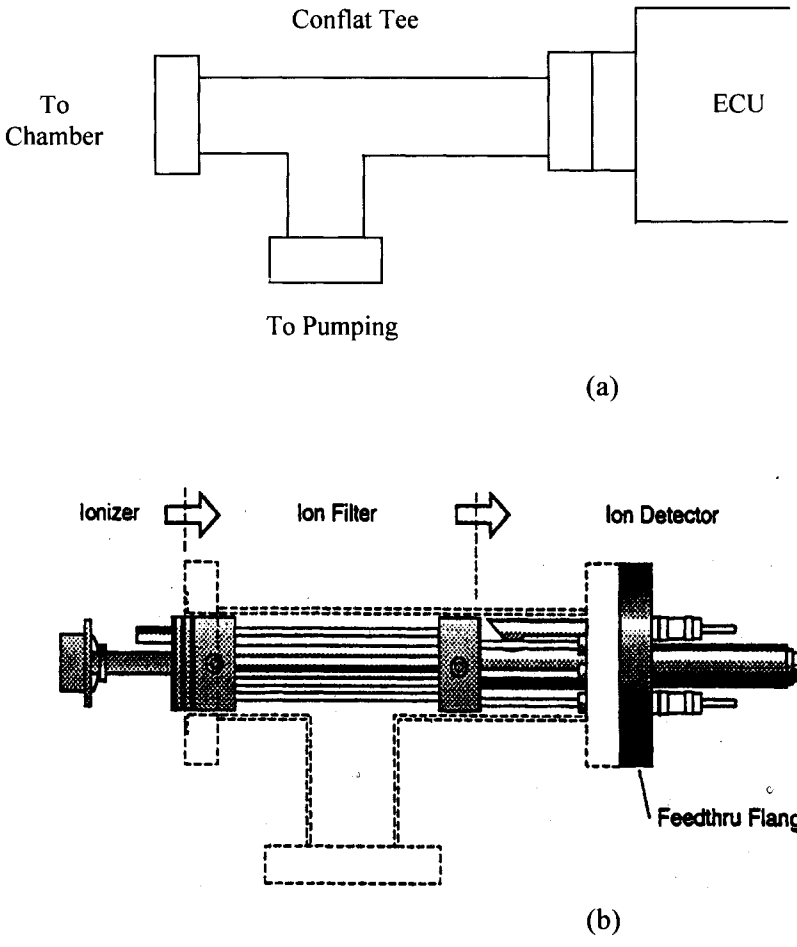

Figure 3.4. CIS analyzer [22].

The quadrupole mass filter is comprised of four electrically conducting cylindrical rods. The rods are held in quadrature and parallel to each other by alumina spacers. The rods are arranged to minimize the distortion of the electrodynamic quadrupole field. The electric field within the rods is created by applying a combination of radio frequency (RF) and direct current (DC) voltages to each pair of the rods as shown in Fig. 3.5. The applied RF frequency is 2.7648 MHz. Positive ions travel through the filter along the z-axis and oscillate in the X and Y directions due to the quadrupole fields. The RF and DC voltages are set to some values that will allow only ions of interest to have stable trajectories. Only those ions will be transmitted to the other end of quadrupole. By varying the DC and RF voltages, different mass-to-charge ratio ions are transmitted at a time. The ECU automatically varies the RF and DC voltages to the necessary values to scan the entire mass spectrum.

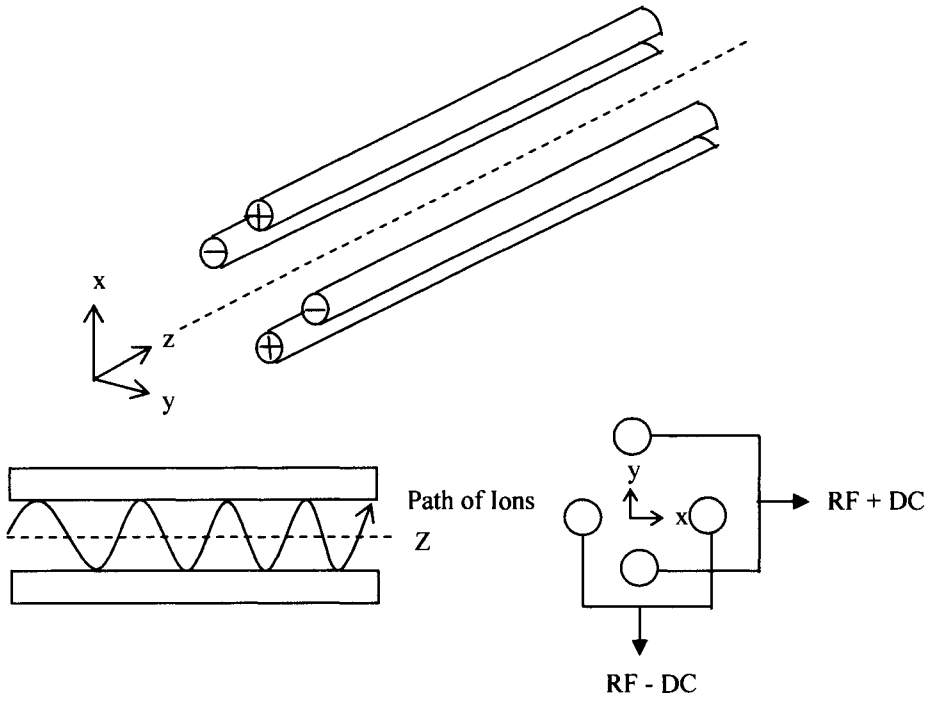

Figure 3.5. Schematic of quadrupole mass filter.

The ions that are successfully transmitted to the end of quadrupole filter enter the ion detector. The detector is shielded from the quadrupole field by a grounded exit plate. The detector used is a stainless steel Faraday cup (FC) located along the Z-axis at the end of the quadrupole. The ions enter the detector, strike the metal wall and extract electrons from the metal. An electrical current is created as a result of this process. The current is transmitted through an RS232 cable to the computer system. The partial pressure of ions is calculated by multiplying the current with the nominal sensitivity of the CIS analyzer. The sensitivity of the analyzer used in this experiment is in the order of 10^{-6} A/Torr. The FC detector's efficiency is the same for all ions regardless of their mass.

3.3 Langmuir Probe

A Langmuir probe is also used in this experiment to support the data obtained from both MS and OES. A diagram of the Langmuir probe is shown in Fig. 3.6. The probe tip is placed inside the plasma chamber, in the close proximity to the substrate. The probe is connected to the DC power supply with a coaxial cable through a feedthru flange. A current meter is placed between the probe and the DC power.

By grounding the chamber wall and applying voltage to the probe, a potential between the probe and the wall is developed inside the chamber. Depending on the voltage applied, electrons from the plasma will be attracted or repelled from the probe tip. Langmuir probe theory is developed based on the assumption that the probe does not disrupt the plasma. It also assumes that all the electrons and ions that enter the plasma sheath are collected by the probe [15]. The sheath is a non-neutral region between plasma and wall or between plasma and foreign object inserted into the plasma.

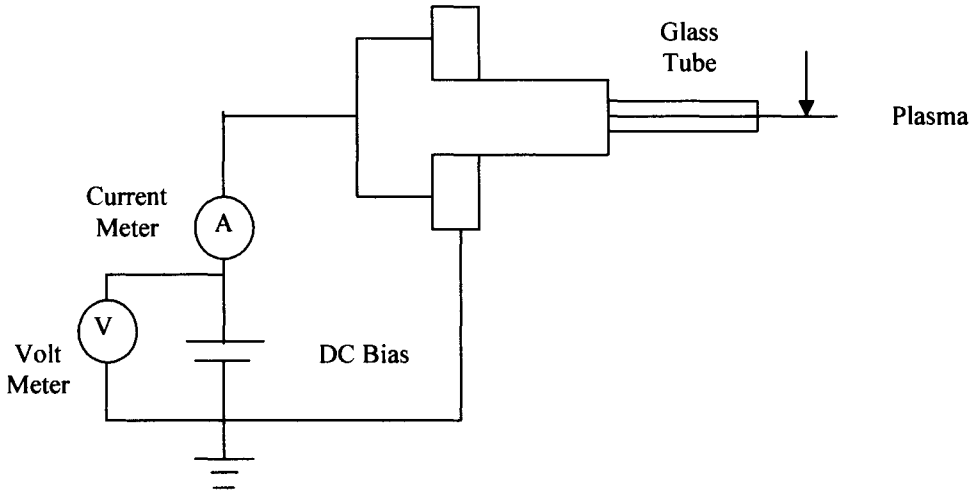

Figure 3.6. Schematic of the Langmuir probe system.

An example of the Langmuir probe data is shown in Fig. 3.7. As shown in Fig. 3.7, the I-V curve generated from the Langmuir probe data consists of three regions: ionic region, transition region and electronic region. When large negative bias is applied to the probe, electrons are repelled and ions are collected on the probe. This is called the ionic region (region 1). In this region, the collected current is due to the thermal motion of ions. On the other hand, when large positive bias is applied, the electrons are attracted and ions are repelled from the probe. The collected current in this electronic region (region 3) is due to the thermal motion of electrons. A transition region (region 2) exists in between the ionic and electronic regions.

The voltage where the current goes to zero is called the floating potential while the point where the probe is at the same potential as the plasma is called the plasma potential. At plasma potential, the current collected by the probe is due to the thermal motion. Because

the thermal velocity of electrons is much higher than the thermal velocity of ions, the current collected by the probe is mainly due to electrons.

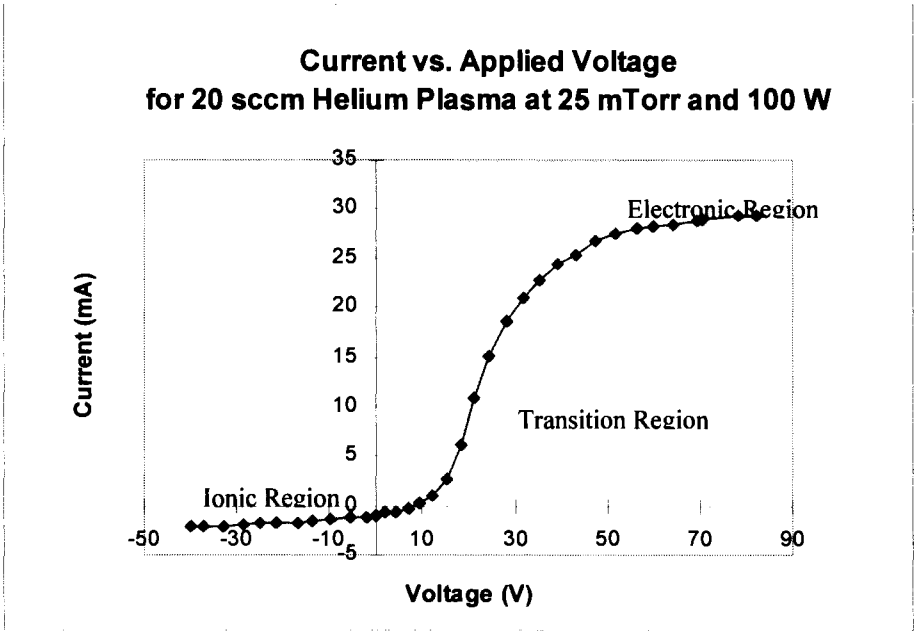

Figure 3.7. Langmuir probe I-V data.

3.4 UV/VIS/NIR Photospectroscopy

To correlate the plasma condition with film growth rate, amorphous silicon films are grown on glass substrate. The film thickness is measured using a Perkin-Elmer dual beam spectrophotometer. The film is mounted perpendicular to the incoming light beam. As the monochromatic beam passes through the sample, part of the light will be reflected and part of it will be transmitted. The interaction between the reflected and transmitted light in the film will cause destructive or constructive interference that occurs when

$$2t\sin\theta = \frac{m\lambda}{n} \tag{3.6}$$

where t is the film thickness, θ is the incident angle, λ is the wavelength, m is an integer and n is index of refraction. The thickness of the film can be calculated from the wavelengths of two adjacent peaks or valleys:

$$t = \frac{\lambda_1 \lambda_2}{2n(\lambda_1 - \lambda_2)} \tag{3.7}$$

where λ_1 and λ_2 are the wavelengths of the adjacent peaks, and n is the index of refraction halfway between λ_1 and λ_2. For the calculation, we will assume n to be constant. Therefore it is important to use λ_1 and λ_2 from the region where the variation on n is small. For this experiment, the interference peaks use to determine film thickness are in the range of 1500 to 2500 nm.

The Perkin-Elmer spectrophotometer is also used to measure the absorption coefficient. Since absorption occurs when the energy of the incident photon is higher than the bandgap of the material, the plot of absorption coefficient versus energy can be used to determine the optical bandgap of the film. Absorption and transmission are defined as

$$A(\lambda)) = \log_{10}\left(\frac{1}{T(\lambda)}\right) \tag{3.8}$$

$$T(\lambda) = [1 - R(\lambda)]^2 \exp[-\alpha(\lambda)t] \tag{3.9}$$

where A(λ) is the absorption, T(λ) is the transmission and R(λ) is the reflection. Substituting equation 3.9 into equation 3.8 and solving for α(λ) gives

$$\alpha(\lambda) = \frac{2.303A(\lambda) - \ln\left[(1 - R(\lambda))^{-2}\right]}{t} \tag{3.10}$$

The absorption coefficient can then be calculated by measuring A(λ) and R(λ). The relationship between the optical bandgap and the absorption coefficient is given by

$$\sqrt{\alpha(\lambda)h\upsilon} = B\left(h\upsilon - E_g\right) \tag{3.11}$$

where B is a proportionality constant and E_g is the Tauc gap [23]. Figure 3.8 shows an example of a plot of $(\alpha \,.\, E_{ph})^{1/2}$ versus E_{ph}. By extrapolating the linear portion of the graph down to the x-axis, we can determine the Tauc gap.

The bandgap can also be estimated using the E^{04} method (Fig. 3.9). The energy when the absorption coefficient is equal to 10^4 is the E^{04}.

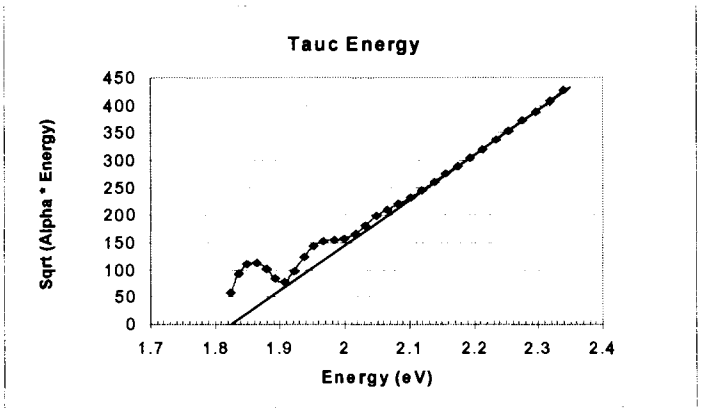

Figure 3.8. Plot of $(\alpha \,.\, E_{ph})^{1/2}$ versus E_{ph} for a:Si film.

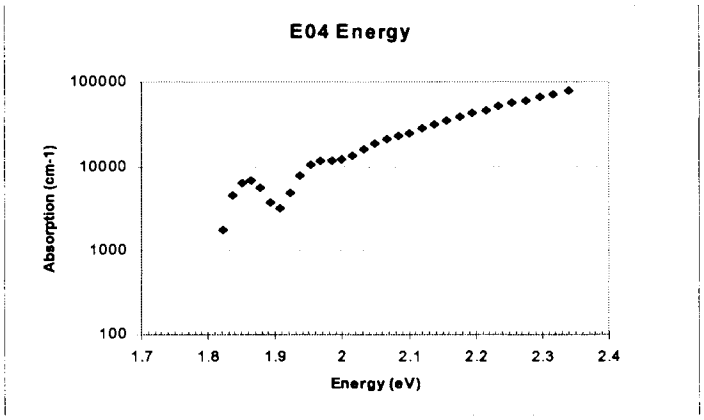

Figure 3.9. Absorption coefficient versus energy plot for a: Si film.

3.5 Photosensitivity

Before electrical measurements are taken, chromium is evaporated on the sample through a mask. The results are two coplanar contacts with L/W ratio of 20. On top of the Cr contacts, silver paint is applied to reduce contact resistance and thus provides good contact with the metal probe.

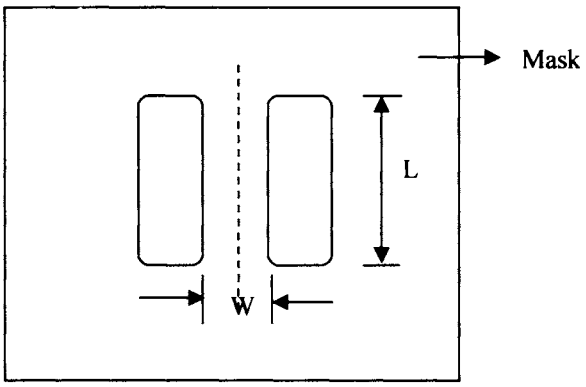

Figure 3.10. Mask used to evaporate Cr contacts on the film.

After the metal contacts are formed, the film is now ready for conductivity measurement. The sample is placed in a light-tight box with a fan directed to the sample to keep it cool during illumination. One-sun light source is used to illuminate the sample. During illumination, the absorbed photons excite carriers to the band edges, creating photo current. In this experiment, the photo current is measured 30 seconds after the sample is illuminated. The lamp is then turned off and the box is closed. The dark current is measured an hour later, after most of the light induced carriers have recombined.

The photo and dark conductivities are calculated using the following equation:

$$\sigma_{ph,d} = \frac{W}{L}\frac{I_{ph,d}}{Vt} \tag{3.12}$$

where V is the applied voltage, t is the film thickness , I is the photo or dark current and W/L is the width to length ratio of the metal contacts. The photosensitivity is calculated by taking the ratio of the photo to dark conductivity. Photosensitivity is a measure of how well the film can collect the photogenerated carriers. Photons are absorbed more efficiently in amorphous material than in crystalline material. More carriers are generated in amorphous films, therefore the photosensitivity of amorphous film is larger that that of crystalline film.

CHAPTER 4. RESULTS

4.1 OES and Mass Spectrometry

OES and mass spectrometry give useful information on how plasma parameters affected the plasma. A change in plasma parameters changes the composition or energy of the ions and atoms in the plasma. In this section we will take a close look on how power, pressure, gas dilution and substrate bias affect the plasma. This information will then be used in the next section to establish a relationship between plasma conditions and film growth rate.

For the OES study, the presence of hydrogen molecules, hydrogen atoms, helium, silicon, and silyl are detected by their emission spectra at 612.2 nm (H_2), 656.3 nm(H_α), 388.8 nm (He), 288.2 nm (Si), and 414.2 nm (SiH) respectively. The Table of Spectral Lines of Neutral and Ionized Atoms [24] and The Identification of Molecular Spectra [25] were extensively used for peak identification.

The OES scan increment was set to 0.02 nm to provide better resolution for the peak of interest. The small scan increment is also necessary to obtain the exact peak location and intensity. Figure 4.1 shows a comparison between OES scan with 0.2 nm and 0.02 nm increments. The scan with 0.2 nm increment gives a false peak at 319 nm. The actual peak at 318.9 nm is seen from the scan with0 .02nm increment.

For the mass spectrometer, peaks at 2 and 3 amu are used to identify H_2 and H_2/H ions (Fig. 4.2), peak at 4 amu is used to identify He ions and peaks at 28, 29, and 31 amu are used to identify Si, SiH, and SiH_3 ions. At the beginning of a scan, the applied DC potential is small (or zero) resulting in a weak electric field along the quadrupole filter. This weak electric field allows unstable ion trajectories to be transmitted through the filter, producing an

output signal called "zero blast". Due to the zero blast condition, the SRS CIS system used for this experiment has been set to zero to prevent zero DC voltage. This means that any peak below 1.5 amu can not be properly detected [15]. Therefore, the peak at 3 amu is used to identify H ions.

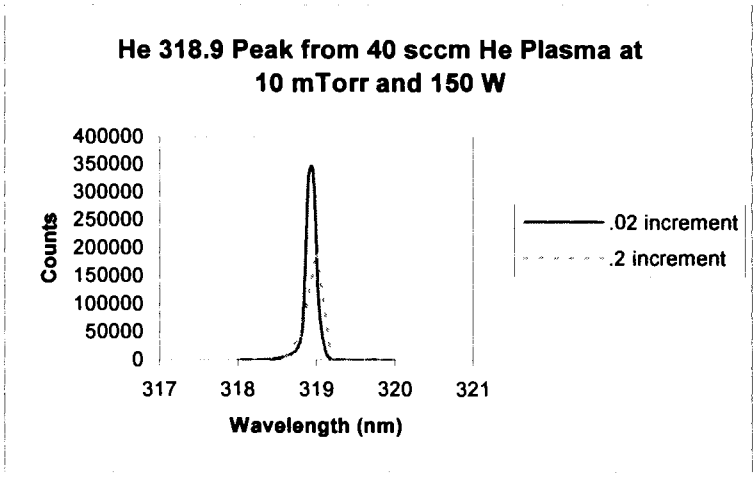

Figure 4.1. Comparison between OES scans with 0.2 and 0.02 nm scan increments.

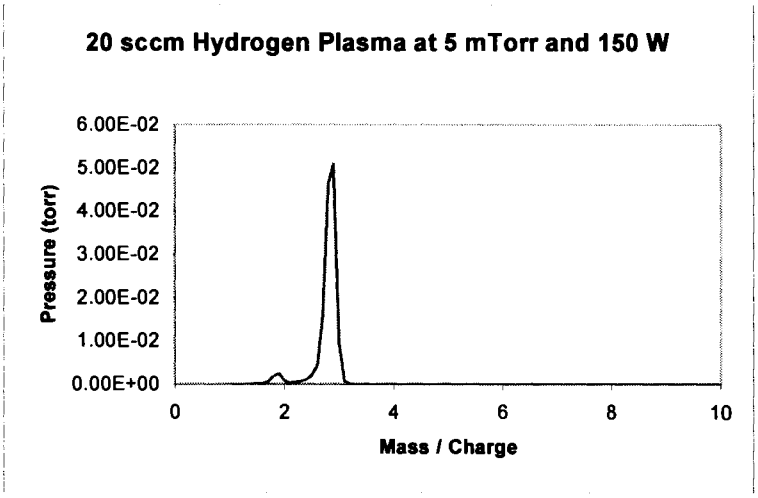

Figure 4.2. An example of mass spectroscopy scan for hydrogen plasma.

4.1.1 Power Effect

OES, MS and Langmuir probe measurements have been taken to evaluate the effect of incident microwave power to the plasma. The OES and MS measurements were collected simultaneously for 20:2:2 helium-hydrogen-silane plasma at 5 mTorr. Figure 4.3 shows OES counts as a function of power. It shows that the emission intensity increases as the power increased. At higher power, more energetic electrons are produced. The interaction between the highly energetic electrons and the atoms or molecules produces more excited species and thus increases the probability for stimulated emission. This results in higher emission intensity.

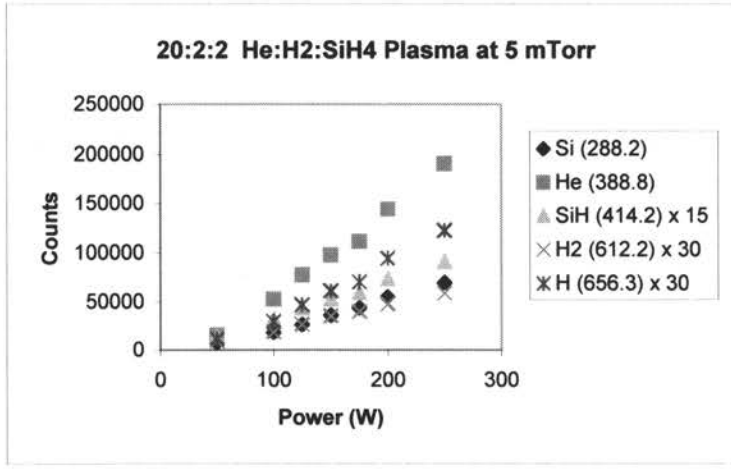

Figure 4.3. OES counts as a function of incident microwave power.

As shown in Figure 4.4, the Langmuir probe measurements support the results from the OES measuremenst. The increase in the incident power results in an increased electron temperature, T_e. The increase in T_e indicates that higher energy electrons are generated. This agrees with previous findings [15], [26]. The highly energetic electrons produce not

only more excited species, but also more radicals and ions. Figure 4.5 shows that the ratio of H atoms to H_2 molecules increases with power. In addition, the MS data indicates an increase in He^{2+}, $H_2^+$and H_2/H^+ ions, when the microwave power is increased from 50 W to 200 W (Fig. 4.6). Increasing the power from 200 W to 250 W did not further increase the

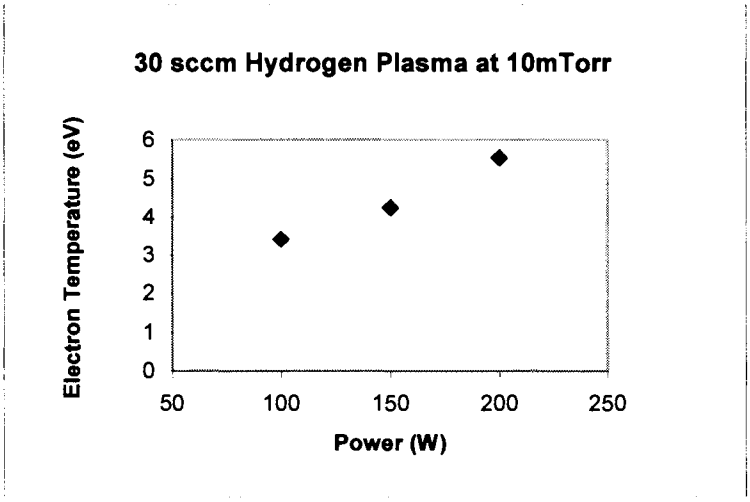

Figure 4.4. Langmuir data showing the effect of power on electron temperature.

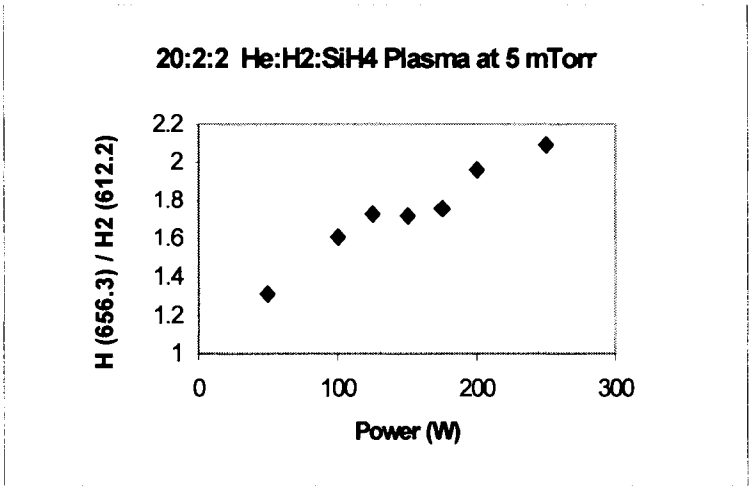

Figure 4.5. The effect of power on ratio of H atoms to H_2 molecules.

detected concentration of He^{2+}, H_2^+ and H_2/H^+ ions. For comparison, MS scans were also collected for 20:2 helium-hydrogen plasma at 5 mTorr. The results, plotted in Fig. 4.7, agree with the data shown in Fig. 4.6. The detected ions increase exponentially when the microwave power is varied from 50 W to 200 W. Increasing the power from 200 W to 250 W does not change the ions concentration.

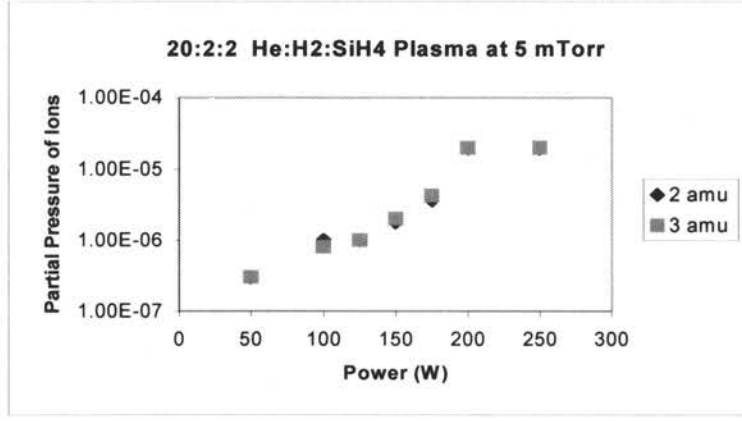

Figure 4.6. He^{2+} and/or H_2 (2 amu) and H_2/H^+ (3 amu) ions in He-H_2-SiH4 plasma as a function of power.

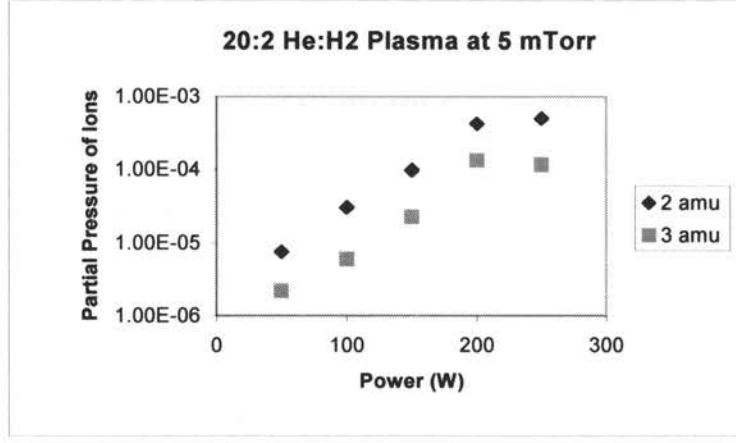

Figure 4.7. He^{2+} and/or H_2^+ (2 amu) and H_2/H^+ (3 amu) ions in He-H_2 plasma as a function of power.

4.1.2 Pressure Effect

The effect of pressure on the plasma was studied using OES, MS and the Langmuir probe. The variation of OES counts with pressure for a He-H_2-SiH_4 plasma at 150 W is shown in Fig. 4.8. In general, the OES counts decrease as the pressure increases. This can be explained by the decrease in the electron temperature measured by the Langmuir probe, shown in Fig. 4.9. When the pressure increases, the mean free path decreases, causing less energetic collisions. As mentioned earlier, only collisions with a certain amount of energy transferred can result in photon emission. The less energetic collisions will not have high enough energy to emit a photon and thus can not be detected by the OES system.

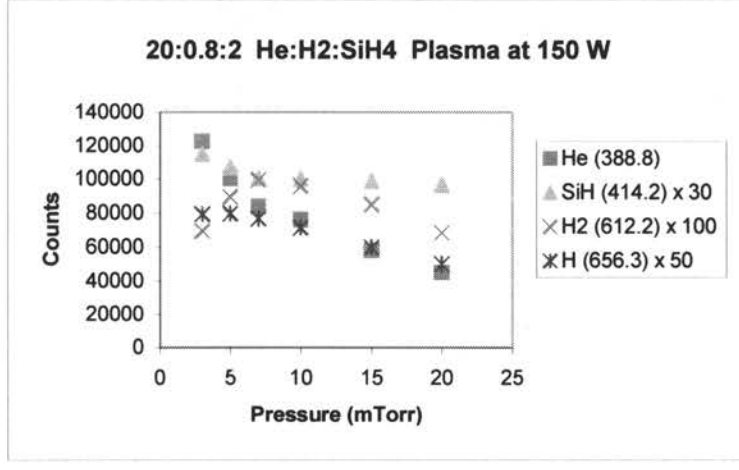

Figure 4.8. OES counts as a function of pressure for He-H_2-SiH4 plasma at 150 W.

Figure 4.8 shows that both of helium and hydrogen atoms counts decrease as the pressure increases. However for H_2 molecules, the EOS count increase for pressure between 3 to 7 mTorr and decreases for pressure above 7 mTorr. At low pressure the dissociation of H_2 molecules to H atoms is more effective, resulting in high H_α / H_2 count ratios. Figure 4.10

shows that the ratio of H alpha to H_2 molecules decreases as the pressure increases. This implies that the dissociation rate of H_2 molecules to H atoms is higher at low pressure.

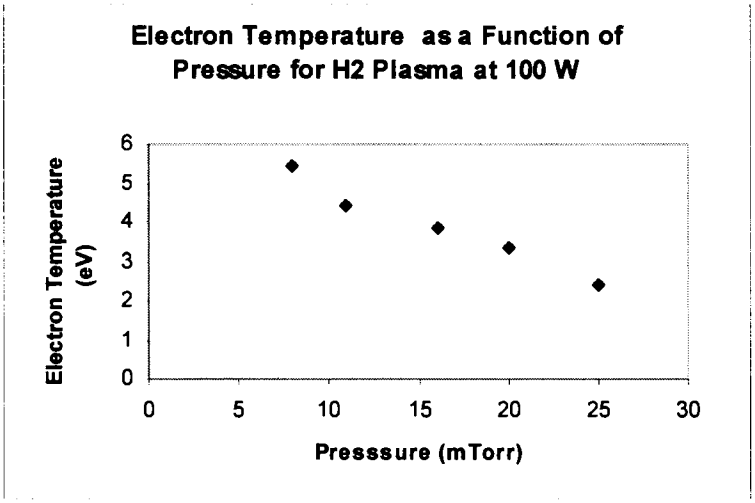

Figure 4.9. Electron Temperature as a function of chamber pressure.

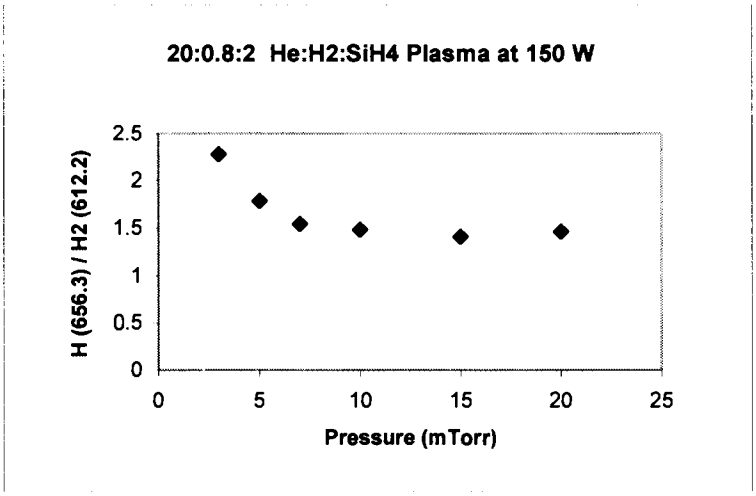

Figure 4.10. Ratio of H alpha to H_2 molecule counts for He-H_2-SiH4 plasma at 150 W.

An increase in pressure also decreases the electron concentration in the plasma, as shown in Fig. 4.11. This result has been noted before [15]. The decrease in electron concentration decreases the collision probability between electron and molecules and thus decreases the concentration of ion formed. Figure 4.12 shows the relationship between the ion concentration and the pressure.

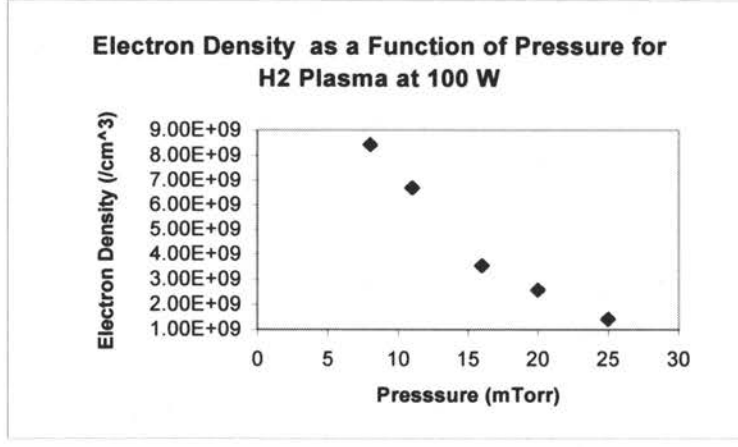

Figure 4.11. Electron density as a function of pressure for H_2 plasma.

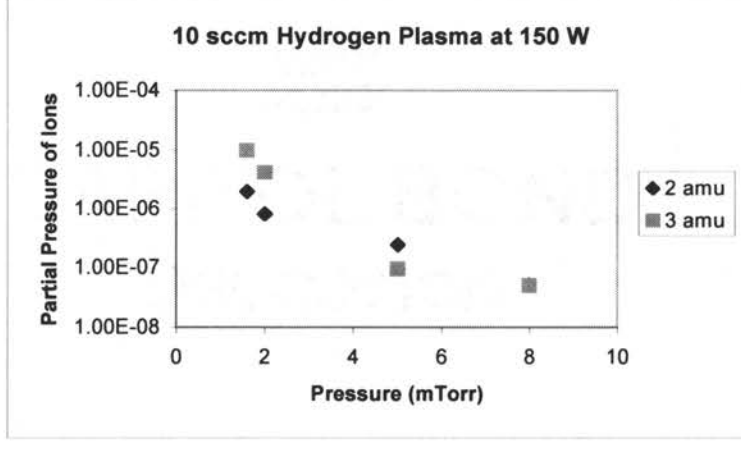

Figure 4.12. H_2^+ (2 amu) and H_2/H^+ (3 amu) ions in H_2 plasma as a function of pressure.

4.1.3 Dilution Effect

The effect of adding silane to a helium plasma is shown in Fig. 4.13. The experiment was conducted by adding small amount of silane to a helium plasma while maintaining a constant chamber pressure. As shown in Fig. 4.13, at 0% silane the OES counts for H_α and H_2 molecules are very low. Adding 1 to 4 sccm silane to a 20 sccm helium plasma results in the increase in Si (288.2nm), H_α (656.3 nm) and H_2 (612.2 nm) counts. As expected, the helium count decrease as the fraction of SiH_4 to He inlet flow increases. As the silane dilution increases, the amount of helium present in the chamber decreases and thus decreases the decomposition rate of silane by helium atoms/ions. The ratio of H_α to H_2 decreases from 2.16 to 1.90 as the silane dilution increases from 5% to 20 % (shown in Fig. 4.14).

OES and MS studies were also conducted to investigate the effect of adding hydrogen to a helium-silane plasma. The plot of OES counts versus H_2 / ($He+SiH_4$) dilution ratio is shown in Fig. 4.15. The OES signals due to excited H_2 (612 nm) and H_α (656.3 nm) ions

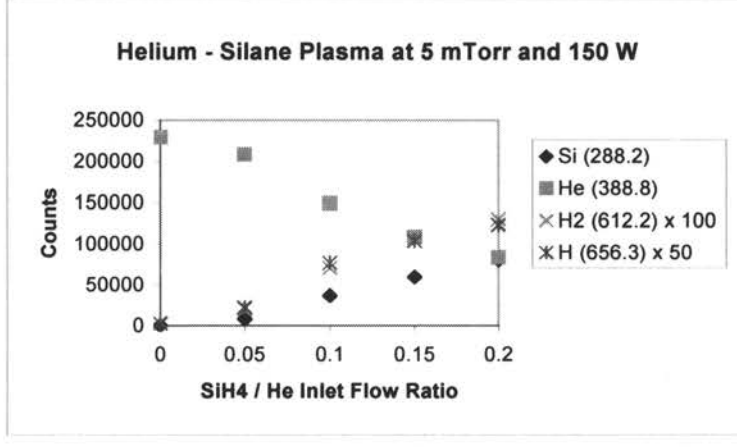

Figure 4.13. EOS counts versus SiH_4/He dilution ratio.

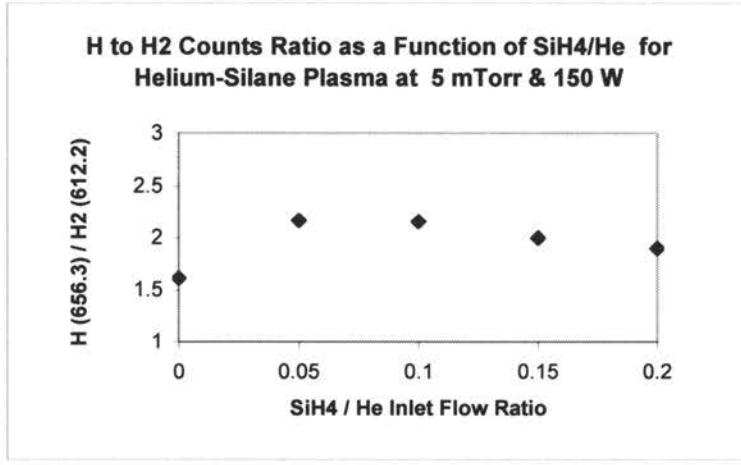

Figure 4.14. H_α to H_2 counts ratio as a function of SiH_4/He dilution ratio.

increase as has been expected. Figure 4.15 also shows that hydrogen dilution reduces the OES counts for He (388.8 nm), Si (288.2 nm) and SiH (414.2 nm). The decrease in SiH signals indicates that the addition of hydrogen reduces the formation of radical responsible for growth. Figure 4.16 shows that the concentrations of Si^+ (28 amu) and SiH^+ (29 amu)

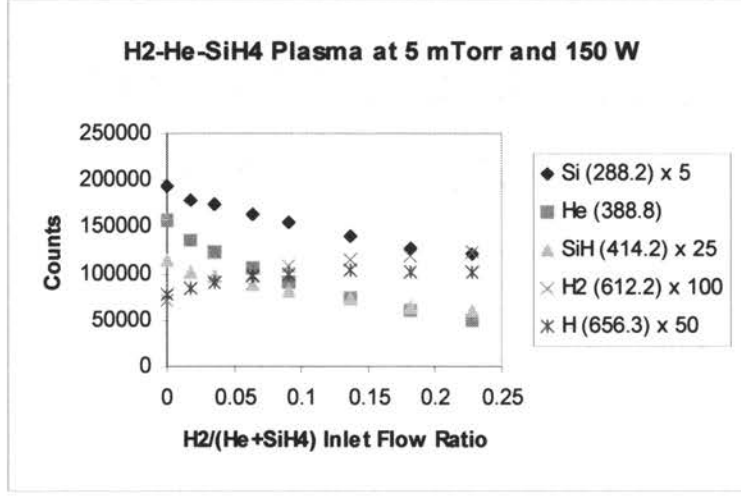

Figure 4.15. OES counts as a function of H_2/(He+SiH_4) dilution ratio.

ions decrease as the hydrogen dilution ratio increases. In addition, hydrogen atom to hydrogen molecule count ratios also decrease with an increase in hydrogen dilution ratio (shown in Fig. 4.17). The correlation between the H_α/H_2 counts ratio and film growth rate will be discussed in section 4.2.

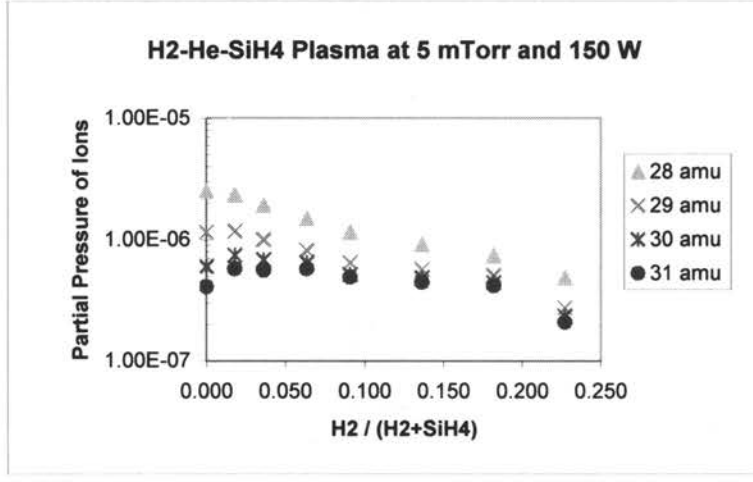

Figure 4.16. Partial pressure of Si^+, SiH^+, SiH_2^+ and SiH_3^+ ions as a function of $H_2/(He+SiH_4)$ ratio.

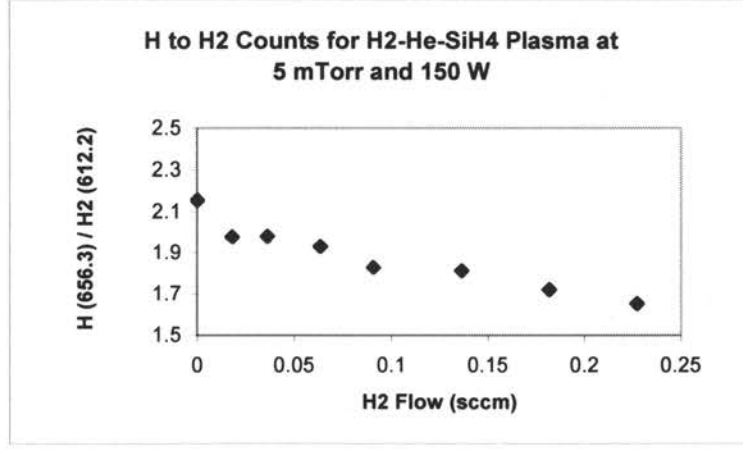

Figure 4.17. H_α to H_2 molecule ratio as a function of $H_2/(He+SiH_4)$ dilution ratio.

4.1.4 Bias Effect

To study the effect of substrate bias, an in-line mass spectrometer was used to detect the ion density in the plasma. A grounded screen was placed in front of the substrate to minimize the effect of bias on the rest of the plasma. The change in partial pressure of ions as a function of bias is shown in Fig. 4.18. The result is the opposite of what would have been predicted. The ion flux increases with substrate bias. This might be due to the increase in plasma potential with bias as was observed for a system without a grounded screen (Fig. 4.19). A similar result was observed before [26]. The increase in ion flux with bias indicates that the geometry of the ground planes in the plasma changes, even with the presence of a grounded screen. The mass spectroscopy result for a system without a grounded plane is shown in Fig. 4.20. Comparing Fig. 4.18 to Fig. 4.20, we found that both systems, with and without grounded plane, show similar results.

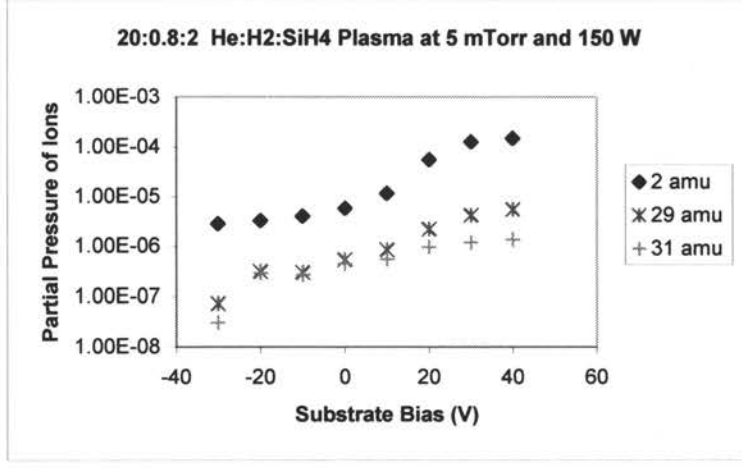

Figure 4.18. Partial pressure of ions versus substrate bias for He-H_2-SiH_4 plasma with a grounded screen.

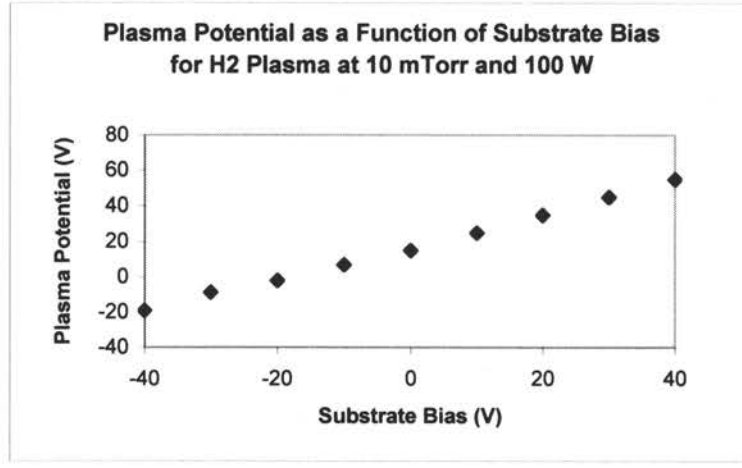

Figure 4.19. Plasma potential as a function of substrate bias.

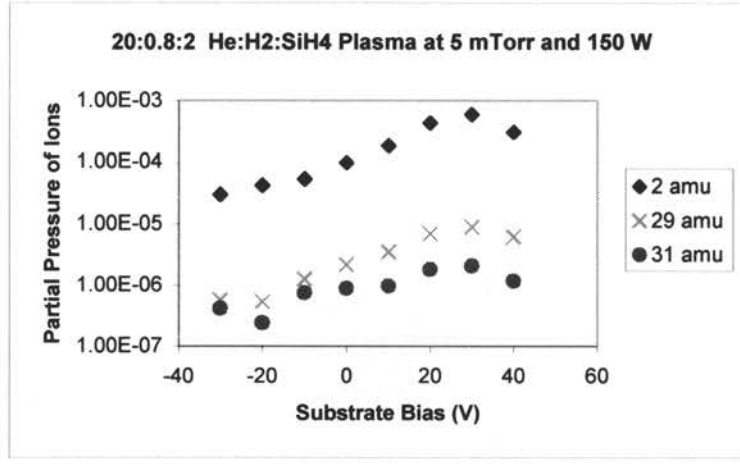

Figure 4.20. Partial pressure of ions versus substrate bias for He-H_2-SiH_4 plasma without a grounded screen.

OES was also used to study the effect of substrate bias on the plasma. The study was conducted on the system without a grounded screen. A typical emission intensity versus bias plot is shown in Fig. 4.21. This plot shows a very interesting result. Unlike the ion flux, the emission intensity does not change much with substrate bias. This can be explained using the

plasma potential versus bias plot. As shown in Fig. 4.19, the plasma potential increases with bias. However, the difference between the plasma potential and substrate bias is almost unchanged. This potential difference is the one seen by the atoms or molecules. Therefore, changing the substrate bias alone does not change the emission intensity. A similar result was also observed for a system with a grounded screen (Fig. 4.22).

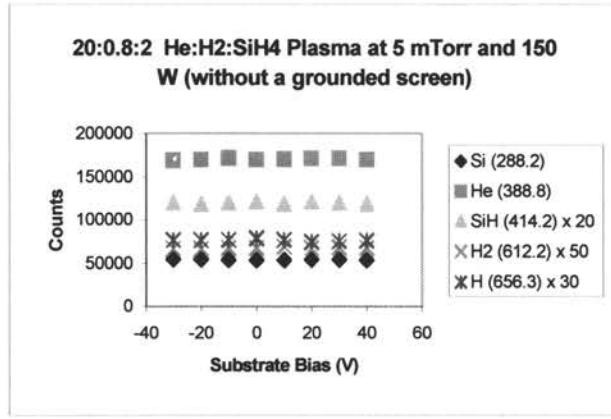

Figure 4.21. Emission intensity versus bias for a system with no grounded screen.

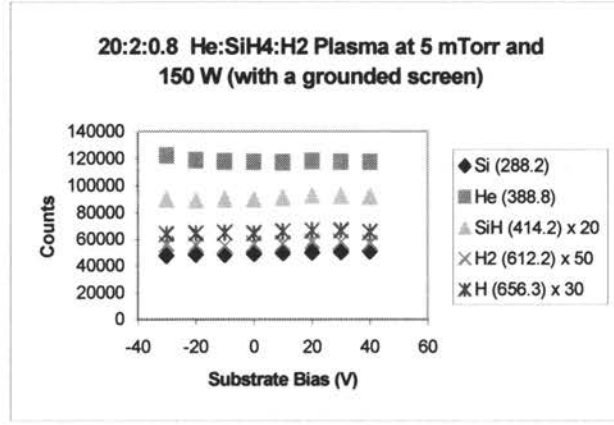

Figure 4.22. Emission intensity versus bias for a system with a grounded screen.

4.2 Film Growth

To determine the effect of plasma parameters on the film growth rate, a series of a-silicon films were grown on glass substrates. The deposition conditions of the samples are listed in Table 4.1. All samples were grown at 350°C and 15 mTorr. The microwave power was kept constant at 75 W. The helium and silane flow rates were maintained at 20 and 4 sccm respectively, while the hydrogen flow rate was varied from 0 to 20 sccm.

The electrical and optical properties of the grown films are listed in Table 4.2. The film thickness decreases from 1.316 to 0.85 μm as the H_2 flow rate increases from 0 to 20 sccm. The Tauc gap and E^{04} are similar for all samples, suggesting that the bandgap remains unchanged. The photosensitivity is in the order of 10^5 to 10^6, indicating an amorphous film.

Table 4.1. Deposition conditions of the a:Si films.

Sample #	Power (W)	Pressure (mT)	He (sccm)	H2 (sccm)	SiH4 (sccm)	Growth Time (min)
3/857	75	15	20	0	4	60
3/862	75	15	20	0.8	4	60
3/863	75	15	20	1.4	4	60
3/858	75	15	20	2	4	60
3/859	75	15	20	5	4	60
3/860	75	15	20	10	4	60
3/861	75	15	20	20	4	60

Table 4.2. Film characteristics.

Sample #	Growth Rate (A/s)	E tauc (eV)	E04 (eV)	Light Conductivity (S/cm)	Dark Conductivity (S/cm)	Photo Sensitivity
3/857	3.656	1.82	1.98	4.71E-06	6.99E-12	6.74E+05
3/862	3.562	1.82	1.97	1.03E-05	4.21E-11	2.44E+05
3/863	3.423	1.83	1.98	9.25E-06	3.08E-11	3.00E+05
3/858	3.291	1.83	1.97	2.78E-05	1.80E-10	1.55E+05
3/859	3.169	1.82	1.97	1.67E-05	4.56E-11	3.65E+05
3/860	2.676	1.82	1.97	1.87E-05	2.78E-11	6.72E+05
3/861	2.362	1.83	1.97	1.06E-05	1.91E-11	5.56E+05

Figure 4.23 shows the effect of hydrogen dilution on growth rate. As the hydrogen flow increases from 0 to 20 sccm, the growth rate decreases from 3.66 to 2.36 A/sec. The decrease in growth rate is due to the decrease in the concentration of radicals responsible for growth. In section 4.1.3 we have shown that H_2 dilution decreases both SiH emission signal (Fig. 4.15) and SiH ion concentration (Fig. 4.16). The correlation between growth rate and SiH emission intensity is shown in Fig. 4.25. The growth rate increases as SiH counts increases. This means that the growth rate depends on the decomposition of silane into its radicals (e.g. SiH_3, SiH_2, SiH and Si). It does not necessarily mean that SiH is the dominant radical responsible for growth. It only implies that the dominant radical is produced at a rate proportional to the rate of production of SiH. Previous work by Gallagher [7,16] showed that SiH_3 was the dominant radical in glow discharge. Further study needs to be done to find out if SiH_3 is the dominant radical in ERC system. Figure 4.25 shows the correlation between growth rate and H/H_2 emission intensity ratio. The increase of growth rate with H/H_2 ratio

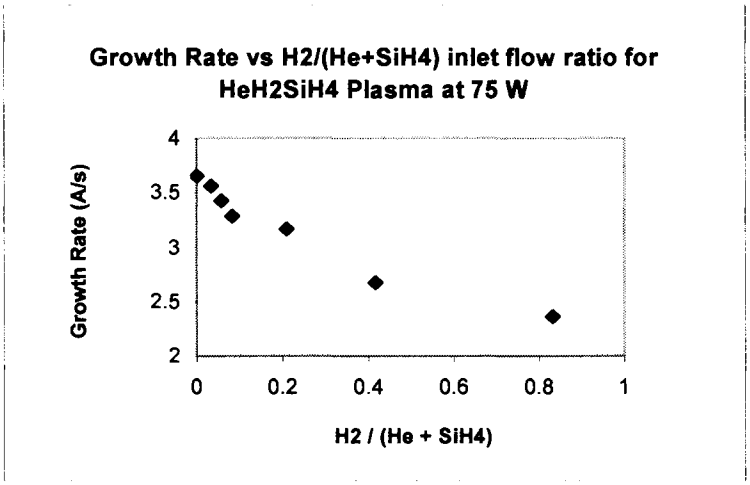

Figure 4.23. Growth rate as a function of H_2 / ($He+SiH_4$) inlet flow ratio.

indicates that growth rate depends on the formation of H ions. At low H/H_2 ratio, a small increase in H ion concentration increases the growth rate. Further increase in H ion concentration increases the sample etch rate and thus slows the growth rate down.

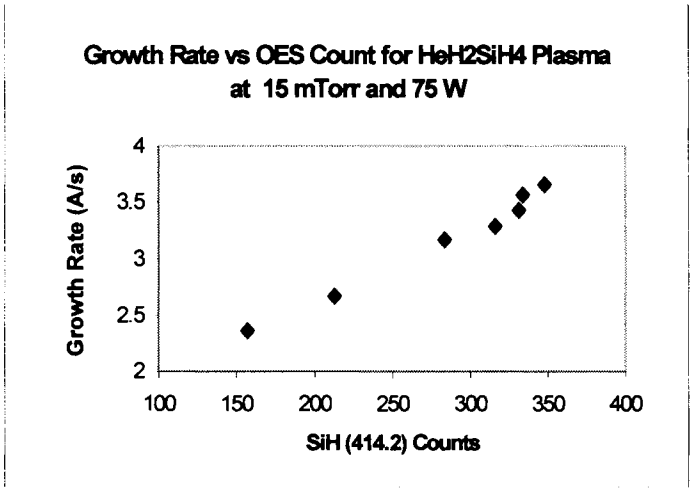

Figure 4.24. Growth rate versus SiH emission intensity.

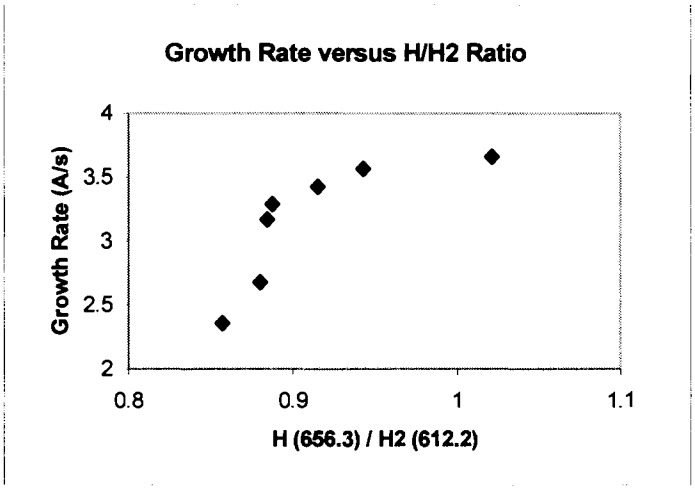

Figure 4.25. Growth rate versus H(656.3) / H_2(612.2) counts ratio.

CHAPTER 5. CONCLUSIONS

The first part of this research focused on plasma characterization using Langmuir probe, optical emission spectroscopy (OES), and in-line mass spectrometry (MS). The effect of microwave power, chamber pressure, gas dilution, and substrate bias on ECR plasma composition was investigated by taking OES and MS measurements simultaneously. Langmuir probe data were used to support the OES and MS findings.

As predicted, the increase in the incident microwave power increases the atomic and molecular emission intensity as well as the ion concentration. This can be explained by the increase in electron temperature. As the electron temperature increases, more energetic collisions are produced and more excited radicals and ions are generated. Similar results were seen by DeBoer [7] and deFreese [19]. As power increases, H_α/H_2 counts ratio also increases. This result indicates that H atom plays a role in growth chemistry.

An increase in pressure reduces the emission counts, ion concentrations and electron temperature. When the pressure increases, the mean free path decreases. The decrease in mean free path produces less energetic collisions and thus creating fewer ions and radicals. The increase in pressure also reduces H_α/H_2 counts ratio. This means that the decrease in pressure produces more H ions/radicals and thus promoting the growth of microcrystalline films.

In this work, we investigated both silane and hydrogen dilution effects. Adding silane into helium plasma increases both Si and H emission intensity. As expected, the helium count is inversely proportional to the SiH_4 concentration. Interestingly, the addition of hydrogen reduces the emission intensity for both Si and SiH. Assuming that the radical responsible for growth is produced at a rate proportional to the rate of formation of SiH, then

the decrease in SiH signal indicates that the addition of hydrogen also reduces the formation of radicals responsible for growth.

For the substrate bias study, a grounded screen was placed in front of the substrate to minimize the effect of the bias on the geometry of the ground plane. The result from this study was very surprising. We found that the ion flux increases with substrate bias. This is due to the increase in plasma potential with bias, as was observed before for a system without a grounded screen [19]. This result suggests that the plasma potential still increases, even with the presence of a grounded screen. Unlike the ion flux, the emission intensity does not change much with substrate bias. As bias increases, the plasma potential also increases. However, the difference in plasma potential and the applied bias is almost unchanged. This potential difference is the one seen by the atoms. Therefore changing substrate bias does not change the emission intensity.

The second part of this research was dedicated to correlate the spectroscopy results to the film growth rate. To do this, a series of amorphous silicon films was grown at different hydrogen dilution ratios. The results show that the film growth rate decreases as the hydrogen dilution increases. The decrease in growth rate was found to be linearly dependent on the SiH counts. This implies that the growth rate depends on the decomposition rate of silane into its radicals. This also suggests that the dominant radical responsible for growth is produced at the rate proportional to the rate of formation of SiH.

In conclusion, we have demonstrated that we can use OES and MS to obtain information about plasma composition that can be used to monitor film growth rate. We have shown that adding a small amount of hydrogen to helium-silane plasma reduces radical formation and thus decreases the growth rate. Subsequent increase in hydrogen dilution

further increases the etching of the films, thereby decreasing the growth rate even more. Surprisingly we found that all three ions SiH, SiH_2 and SiH_3 play a major role in growth. SiH concentration can even be higher that SiH_3 concentration as shown in figure 5.1. This contradicts the standard growth model for growth [7].

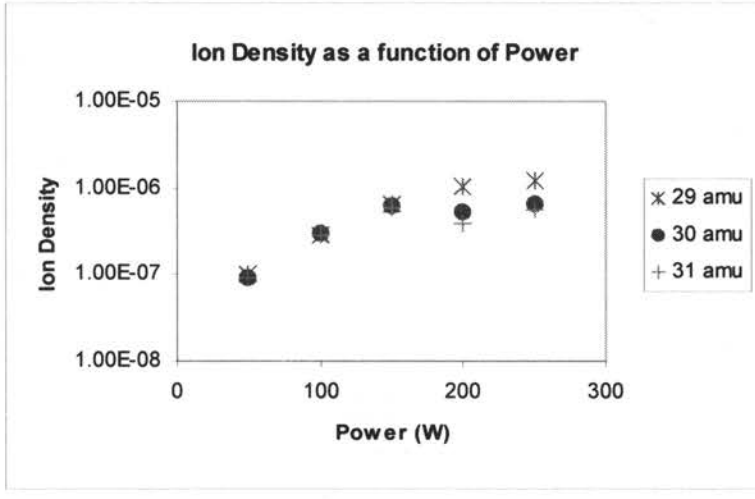

Figure 5.1. SiH, SiH2 and SiH3 ion densities as a function of power.

The work on He-H_2-SiH_4 plasma needs to be continued to determine the dominant radical responsible for growth in the ECR plasma. An ion-beam mass spectrometer can be used to do a compositional analysis of plasma. The details of this measurement technique can be found in a paper by Sz. Katai [27]. Moreover, to better understand the role of hydrogen in the plasma, the loss kinetics of hydrogen can be investigated using a method similar to the one reported by S. Takashima [28]. The OES and MS measurement can also be used to correlate plasma composition with growth rate for different types of film, such as silicon germanium and germanium carbide.

REFERENCES

1. K. Schuegraf, Handbook of Thin-Film Deposition Process and Techniques, Noyes Publications, New Jersey, 1988.

2. J. Hautala, Z. Saleh, J.F.M. Westendorp, H. Meiling, S. Sherman, and S. Wagner, Mat. Res. Soc. Symp. Proc., **420**, 83 (1996).

3. E. Fortunato and R. Martins, Mat. Res. Soc. Symp. Proc., **507**, 303 (1998).

4. R.D. Knox and V.L. Dalal, J. Vac. Sci. Technol., **A9**, 474 (1991).

5. M.C.M. van de Sanden, R.J. Severens, W.M.M. Kessels, R.F.G. Meulenbroeks, and D.C. Schram, J. Appl. Phys., **84**, 2426 (1998).

6. K. Fukutani, T. Sugawara, W. Futako, T Kamiya, C.M. Fortmann, and I. Shimizu, Mat. Res. Soc. Symp. Proc., **507**, 211 (1998).

7. D.A. Doughty, J.R. Doyle, G.H. Lin, A. Gallagher, J. Appl. Phys., **67**, 6220 (1990).

8. V.L. Dalal, E.X. Ping, S. Kaushal, M. Bhan, and M. Leonard, Appl. Phys. Lett., **64**, 1862 (1994).

9. G. Bruno, P. Capezzuto, and A. Madan, Plasma Deposition of Amorphous Silicon-Based Materials, Academic Press, San Diego, 1995.

10. K.E. Lonngren, Introduction to Physical Electronics, Allyn and Bacon, Newton, 1988.

11. R. Payling, D. Jones, and A. Bengtson, Glow Discharge Optical Emission Spectrometry, John Wiley & Sons, New York, 1997.

12. M.A. Lieberman and A.J. Lichtenberg, Principles of Plasma Discharges and Materials Processing, John Wiley & Sons, New York, 1994.

13. O.A. Popov, High Density Plasma Sources, Noyes Publications, New Jersey, 1995.

14. S.M. Rossnagel, J.J. Cuomo, and W.D. Westwood, Handbook of Plasma Processing Technology, Noyes Publications, New York, 1989.

15. S. DeBoer, Ph.D. Dissertation, Iowa State University, 1995.

16. R. Robertson, D. Hils, H. Chatman, and A. Gallagher, Appl. Phys. Lett., **43**, 544 (1983).

17. A. Kono, N. Koike, H. Nomura, and T. Goto, Jpn. J. Appl. Phys., **34**, 307 (1995).

18. M.J. McCaughey and M.J. Kushner, J. Appl. Phys., **65**, 186 (1989).

19. M. Kawase, T. Nakai, A. Yamaguchi, T. Hakozaki, and K. Hashimoto, Jpn. J. Appl. Phys., **36**, 3396 (1997).

20. SpectraPro-300i Operating Instructions, Acton Research Corporation, Massachusetts.

21. L. Ebdon, E.H. Evans, A. Fisher, and S.J. Hill, Analytical Atomic Spectrometry, John Wiley & Sons, Chichester, 1998.

22. Operating Manual and Programming Reference, Stanford Research Systems, Sunnyvale, 1997.

23. B.K. Oliver, M.S. thesis, Iowa State University, 1999.

24. A.R. Striganov and N.S. Sventitskii, Tables of Spectral Lines of Neutral and Ionized Atoms, Plenum Data Corporation, New York, 1968.

25. R.W.B. Pearse and A.G. Gaydon, The Identification of Molecular Spectra, John Wiley & Sons, New York, 1963.

26. M. deFreese, V.L. Dalal and J. Falter, Proc. of MRS, **664**, A5.2 (2001).

27. Sz. Katai, Z. Tass, L. Bori, Gy. Hars, and P. Deak, Rev. Sci. Instrum., **70**, 3324 (2001).

28. S. Takashima, M. Hori, and T. Goto, J. Appl. Phys., **90**, 5497 (2001).

ACKNOWLEDGMENTS

I would like to take this opportunity to acknowledge the various people who have helped, guided and supported me during my research. First, I would express my sincere gratitude to my major professor, Dr. Vikram Dalal, for his support and for making this learning experience possible for me. I would also like to thank Dr. Gary Tuttle and Dr. David Lynch for serving as my committee member.

I would like to thank NREL and NSF for supporting this work. I would also like to thank the department of Electrical Engineering and Graduate College of Iowa State University for the financial support during my first year at the Microelectronics Research Center (MRC).

Thanks go out the people at MRC for their help, support and friendship. Thanks to Kay Han, Max Noack, Roger Keen, Yong Liu and Paul Seberger for their help with the spectrometers and reactor. Thanks to Curtis Sell for helping me with the Langmuir probe. Thanks are also due to Neha Gandhi, who helped taking the measurements and processing the data.

A special thanks goes out to my fiancé, Joe, for his support and encouragement. Thanks are also due to my aunt, Merry for her love and support. Finally, I would like to thank my parents and my brother, Michael for believing in me, loving me and supporting me throughout these years.

The completion of this work would not be possible without the help and support from all of you. Thank you.